Fermi National Accelerator Laboratory

FERMILAB-PUB-87/68-T
April, 1987

Testing Couplings of the Three Vector Bosons Through Hadron Collision at Tevatron Energy

Chao-Hsi Chang[1]
Fermi National Accelerator Laboratory
P.O. Box 500, Batavia, Illinois 60510
and
Department of Physics, The University of Michigan
Ann Arbor, Michigan 48109
and
S.-C. Lee[2]
Fermi National Accelerator Laboratory
P.O. Box 500, Batavia, Illinois 60510

Abstract

A test for vector boson trilinear couplings through hadron collision at Tevatron energy is investigated. The contributions from the standard model to the polarization cross section for W^+W^- pair production process are given and deviations from the standard model are considered. It is pointed out that some effects may be observable in Tevatron collider experiments.

[1] On leave from Institute of Theoretical Physics, Academia Sinica, P.O. Box 2735, Beijing, China (the address after May, 1987).

[2] On leave from Institute of Physics, Academia Sinica, Taipei, Taiwan 11529, China.

Operated by Universities Research Association Inc. under contract with the United States Department of Energy

I. Introduction

Since the weak boson $W^{\pm}$ and Z^{o} were discovered [1], tests of the couplings of $W^{\pm}, Z^{o}$ and γ to see if they are of gauged $SU(2)$ x $U(1)$ symmetry have become one of the most interesting problems [2-29]. It is important not only for proving the standard model [30], but also for testing models beyond [31].

In order to pose this problem, one can focus on experiments at LEP-II in the production of charged weak boson ($W^{\pm}$) pair in $e^{+}e^{-}$ annihilation, which is related to the couplings of $W^{+}W^{-}Z^{o}$ and $W^{+}W^{-}\gamma$. Having relatively higher luminosity (5 x $10^{31} cm^{-2} sec^{-1}$) and being in the clean environment of $e^{+}e^{-}$, undoubtedly LEP-II will give us a lot of useful information on the couplings. However, since the $p\bar{p}$-collider Tevatron has begun to accumulate data, we think it is worthwhile to entertain the possibilities to test these couplings and to investigate what kinds of deviations from the standard model are comparatively easier to be detected in the Tevatron Collider.

Although a hadron collider is not in a clean environment to test these couplings as in $e^{+}e^{-}$, besides having at present a relatively low luminosity to work with, it has some advantages. It was pointed out in ref. [32] that if there are some deviations from the standard model and their effects are proportional to the masses of the fermions in the pair production processes $f\bar{f} \to W^{+}W^{-}$, then it is almost impossible for $e^{+}e^{-}$ collider to observe them. However, for hadron collider it is possible due to heavy quark components in the nucleon structure functions. Another advantage is that in hadron collider the invariant mass of the W pair can reach a relatively high value. We know that the higher the invariant mass, the easier it becomes to test the gauge cancellation and to see the deviations from gauge couplings if there are any. Therefore, under the Tevatron condition, how well one can test the couplings of the three vector bosons deserves a careful analysis. On the other hand, if someone hopes to discover new physics through $W^{+}W^{-}$ production, he also needs to know the standard model contributions as well as possible deviations as a background. Thus, in this paper we will investigate these problems, i.e., considering the Tevatron conditions, we will compute the $W^{+}W^{-}$ production cross sections systematically.

In ref. [32], the authors pointed out that due to heavy quarks, all of the most general couplings of the three vector bosons should be considered in hadron collision

processes where there are ten types in total, as opposed to what the authors of refs. [7,28] did in the e^+e^- collider case where they ignored all couplings if the contributions to the amplitude are proportional to the fermion masses, which certainly is a very good approximation for e^+e^- collision. Moreover, in hadron collision, the Higgs exchange mechanism is not ignorable either for the same reason. In order to be consistent, we also should consider the general couplings of Higgs to the bosons. Thus, in W^+W^- pair production processes through annihilation of a pair of $q\bar{q}$, in general, 23 types of couplings (or, say, form factors) in total will be relevant. The 23 consist of ten for W^+W^-Z vertex, seven for $W^+W\gamma$, three for W^+W^-H (here, the Higgs H couples to quarks as a scalar) and three for $W^+W^-H_P$ (here the "Higgs" H_P couples to quarks as a psuedoscalar). In this paper, we will discuss their effects separately in $p\bar{p}$ collision at Tevatron energy.

Being interested in the three vector boson couplings, we will not touch the related mechanism such as the equivalent W boson fusion mechanism and gluon fusion through fermion loop mechanism, etc. [27,33], since their contributions are incoherent to what we will discuss. Thus, we focus on the W^+W^- pair production through Drell–Yan mechanism [34]. Owing to such a large number of possible couplings, if one wants to obtain any information on the individual coupling, one has to perform a polarization analysis [7,8,25,28].

One may imagine that if one keeps all mass terms, the formalism would be complicated, especially with respect to those couplings which would not contribute in the massless limit. However, in fact, we find that the density matrix can be factorized into four terms so the final results are not so complicated.

This paper is organized as follows: in the next section, the most general couplings for $W^+W^-\gamma, W^+W^-Z^o, W^+W^-H$ and $W^+W^-H_P$ will be given; the density matrix of polarization for W^+ and W^- are derived. In Section III, the formulas of W^+W^- pair production cross sections for $p\bar{p}$ collision are presented. Adopting the EHLQ structure functions [26], and setting the couplings to deviate from those of the standard model predictions one by one, we compute the numerical values of the polarization cross sections and plot the cross sections against the angle between the proton beam and the produced W boson in the hadron center of mass system and against the invariant mass of the W^+W^- pair. In order to compare with the standard model, in every figure we also plot the corresponding standard model

curves. In the last section, Section IV, we will discuss our results and draw some conclusions.

II. General Couplings and Polarization Density Matrix

A. General Couplings of the Three Vector Bosons

The strategy of investigating the couplings for the three boson vertex in a model independent way is to start from the most general Lorentz covarient couplings, which are independent of each other, and then to set each term to a non-standard model value to see its corresponding consequences. Therefore, we first discuss the most general couplings.

In this paper, we restrict ourselves to consider only the W^+W^- pair production, hence, we need the most general couplings for W^-W^+Z and $W^+W^-\gamma$. In ref. [28], the authors considered the process $e^+e^- \to W^+W^-$ in which the masses of the fermions may be ignored so that only fourteen of the most general couplings are effective.[3] As a matter of fact, the most general couplings for the three vector bosons with W^+W^- on shell should involve seventeen couplings. They are

$$\begin{aligned}\Gamma_V^{\alpha\beta\mu}(q_1,q_2,P) &= f_1^V(q_1-q_2)^\mu g^{\alpha\beta} - \frac{f_2^V}{m_w^2}(q_1-q_2)^\mu P^\alpha P^\beta + f_3^V(P^\alpha g^{\mu\beta} - P^\beta g^{\mu\alpha}) \\ &+ if_4^V(P^\alpha g^{\mu\beta} + P^\beta g^{\mu\alpha}) + if_5^V\varepsilon^{\mu\alpha\beta\rho}(q_1-q_2)_\rho \\ &- f_6^V\varepsilon^{\mu\alpha\beta\rho}P_\rho - \frac{f_7^V}{m_w^2}(q_1-q_2)^\mu\varepsilon^{\alpha\beta\rho\sigma}P_\rho(q_1-q_2)_\sigma \qquad (2.1) \\ &+ if_8^V P^\mu g^{\alpha\beta} - i\frac{f_9^V}{m_w^2}P^\mu P^\alpha P^\beta - i\frac{f_{10}^V}{m_w^2}P^\mu\varepsilon^{\alpha\beta\rho\sigma}P_\rho(q_1-q_2)_\sigma\end{aligned}$$

where $\Gamma_V^{\alpha\beta\mu}$ is the vertex of the three bosons (Fig. 1a).

$$< W^-(q_1\lambda_1)W^+(q_2\lambda_2) \mid J_V^\mu \mid 0 >= e_\alpha(\lambda_1)\bar{e}_\beta(\lambda_2)\Gamma_V^{\mu\alpha\beta}(q_1,q_2,P), \qquad (2.2)$$

and V presents γ or Z°. Note that f_8^γ vanishes and $f_9^\gamma, f_{10}^\gamma$ are not indepent of f_4^γ, f_5^γ due to charge conservation. In fact, even if charge conservation is violated,

[3]The authors of ref. [7] had done the same, but as pointed out in ref. [28], they included two more couplings which are not independent of the rest when fermion masses are neglected.

$f_8^\gamma, f_9^\gamma, f_{10}^\gamma$ will not contribute to $f\bar{f} \to W^+W^-$ at all due to the vector coupling of γ to fermion. Therefore, in eq. (2.1), these three would not be included in our discussions. Considering $WW\gamma$ and WWZ, we now have seventeen couplings $f_i^Z (i = 1, 2 \cdots 10)$ and $f_i^\gamma (i = 1, 2 \cdots 7)$. It is easy to check that these f_i^Z and f_i^γ are independent of each other and taking into account the on-shell conditions

$$q_1^2 = q_2^2 = m_w^2, \quad (q_1 e^{\lambda 1}) = (q_2 e^{\lambda 2}) = 0 \tag{2.3}$$

there is no more independent couplings.

In addition to what has been shown for the fourteen couplings in ref. [28], we list the C,P,T, properties of the seventeen couplings in Table 1.

Table 1

i	1-3.	4.	5.	6.7.	8.9.	10.
P	+	+	-	-	+	-
CP	+	-	+	-	+	-
C	+	-	-	+	+	+

In the standard model, non-Abelian gauge invariance gives very strong constraints on the couplings:

$$\begin{aligned} f_1^V(S) &= 1 + 0(\alpha) \\ f_2^V(S) &= 0(\alpha) \\ f_3^V(S) &= 2 + 0(\alpha) \end{aligned} \tag{2.4}$$

and the others are either $0(\alpha)$ or higher order in α. Since we are testing the three vector boson couplings (Fig. 1) through Drell-Yan mechanism [34] (Fig. 2a) and we want to keep the heavy quark mass effects so we also include the related diagram through scalars (Fig. 2c). To test the standard model thoroughly, it is also necessary to test the deviation from the minimum Higgs sector. Therefore, we also generalize the Higgs couplings to the W^+W^- pair. According to the different couplings with or without γ_5 with fermions, the scalar couplings to W^+W^- are denoted as $\Gamma^{\alpha\beta}_{(H)}$, where the scalar couples to fermions without γ_5, and $\Gamma^{\alpha\beta}_{(H_\gamma)}$ where the scalar couples

to fermions with γ_5 through (Fig. 2c). With the definition of the vertex (Fig. 1b)

$$< W^-(\lambda_1 q_1) W^+(\lambda_2 q_2) \mid J \mid 0 >= e_\alpha(\lambda_1) e_\rho(\lambda_1) \ \Gamma^{\alpha\beta}_{(H,H_P)} \tag{2.5}$$

the most general $\Gamma^{\alpha\beta}_{(H)}$ and $\Gamma^{\alpha\beta}_{(Hp)}$ are as follows

$$\Gamma^{\alpha\beta}_{(H)} = f_1^S g^{\alpha\beta} + \frac{f_2^S}{m_w^2} P^\alpha P^\beta + \frac{f_3^S}{m_w^2} \varepsilon^{\alpha\beta\rho\sigma} P_\rho (q_1 - q_2)_\sigma \tag{2.6}$$

and

$$\Gamma^{\alpha\beta}_{(H_P)} = i f_1^P g^{\alpha\beta} + i \frac{f_2^P}{m_w^2} P^\alpha P^\beta + i \frac{f_3^P}{m_w^2} \varepsilon^{\alpha\beta\rho\sigma} P_\rho (q_1 - q_2)_\sigma \ . \tag{2.7}$$

For the standard model

$$\begin{aligned} f_1^S &= 1 + 0(\alpha) \\ f_i^S &= 0(\alpha) \\ f_i^P &= 0(\alpha) \end{aligned} \quad . \tag{2.8}$$

It turns out that the contributions from $\Gamma^{\alpha\beta}_{(H,H_P)}$ are relatively small at Tevatron energy except at the peak of resonances in the W^+W^- channel. Therefore, later on we will not discuss them in this paper, but we still keep them in the formulas so that they can be used to analyze the S–channel resonances.

B. The polarization Density Matrix

In order to determine all the couplings in eq. (2.2), one has to analyze the polarization behavior.

In the hadron collision, the subprocess concerned is $q\bar{q} \to W^+W^-$. To calculate the cross section, we need to consider all diagrams in Fig. 2.a–c. According to the Feymann rules, we can easily write down the scattering amplitude. Neutral current and low-energy experiments indicate that the couplings for the vector bosons (γ, Z) to the fermions (quarks and leptions) should be given by those of the standard model. For definiteness, we assume the scalars H, H_P couple to the fermions in the same way as the Higgs do in the standard model.

Let $M(k_1\sigma_1, k_2\sigma_2; q_1\lambda_1, q_2\lambda_2)$ be the scattering amplitude of $q\bar{q} \to W^+W^-$, k_1, k_2 and σ_1, σ_2 are the momenta and helicities of quark and antiquark respectively, and

q_1, q_2 and λ_1, λ_2 are the momenta and polarization respectively (Fig. 3) for the W bosons. In the paper, we will use the rectangular basis $e^\lambda(q)$ for the polarizations of W and use the conventions of ref. [28] so that $\lambda = 1$ labels the transverse polarization in the production plan, $\lambda = 2$ labels the transverse polarization perpendicular to the production plane, and $\lambda = 3$ labels the longitudinal polarization. The polarization density matrix is defined by

$$P_{\lambda_1\lambda_2;\lambda_1'\lambda_2'} = \sum_{\sigma_1\sigma_2} M\left(k_1\sigma_1, k_2\sigma_2; q_1\lambda_1, q_2\lambda_2\right)\, M^*\left(k_1\sigma_1, k_2\sigma_2; q_1\lambda_1', q_2\lambda_2'\right) \ . \tag{2.9}$$

Through a straightforward calculation, $P_{\lambda_1\lambda_2;\lambda_1'\lambda_2'}$ can be factorized into four terms

$$P_{\lambda_1\lambda_2;\lambda_1'\lambda_2'} \equiv 2e^4 \tilde{P}_{\lambda_1\lambda_2;\lambda_1'\lambda_2'} \tag{2.10}$$

$$\tilde{P}_{\lambda_1\lambda_2;\lambda_1'\lambda_2'} = \mathcal{R}^v_{\lambda_1\lambda_2} R^{v*}_{\lambda_1'\lambda_2'} + \mathcal{R}^a_{\lambda_1\lambda_2} R^{a*}_{\lambda_1'\lambda_2'} + S^v_{\lambda_1\lambda_2} S^{v*}_{\lambda_1'\lambda_2'} + S^a_{\lambda_1\lambda_2} S^{a*}_{\lambda_1'\lambda_2'} \ . \tag{2.11}$$

where $\mathcal{R}^{v,a}_{\lambda_1\lambda_2}$ and $S^{v,a}_{\lambda_1\lambda_2}$ are 3x3 matrices. Here, and later on, the star "$*$" means to take complex conjugate. Because the couplings of $W^+W^-\gamma$ and W^+W^-Z appear in the matrices with certain combinations, we define the following quantities:

$$a_n = Q_i\left(f_n^\gamma - \frac{s}{s-m_z^2} f_n^z\right) \ ; \ b_n = -\left(\frac{L_i - R_i}{2\sin^2\theta_w}\ \frac{s}{s-m_z^2}\ f_n^z\right), \quad {}^{n=1,\cdots,10} \tag{2.12}$$

$$b = \frac{1}{4\sin^2\theta_w} \sum_I^t \frac{s\mid V_{iI}\mid^2}{t-m_I^2} \tag{2.12a}$$

$$b_m^{S,P} = \frac{1}{2\sin^2\theta_w}\ \frac{s}{s - m_H^2 - i\Gamma_H m_H}\ f_m^{S,P} \quad m = 1,2,3 \tag{2.12b}$$

where Q_i are the electric charge of the incoming quark, L_i, R_i their left and right weak charge

$$L_i = \tau_i^3 - 2Q_i\sin^2\theta_w \ , \quad R_i = -2Q_i\sin^2\theta_w \tag{2.12c}$$

m_I are the masses of the corresponding t-channel quarks, V_{iI} are the KMC quark mixing matrix elements, m_H and Γ_H are the mass and widths of the neutral scalars.

The matrices R^v, R^a, S^v and S^a have the following properties

$$A_{12} = A_{21}^* \ , \quad A_{13} = -A_{31}^* \ , \quad A_{23} = -A_{32}^* \tag{2.13}$$

where A represents any one of $\mathcal{R}^v, \mathcal{R}^a, S^v, S^a$ matrices and $a_n, b_n, b, b_m^{S,P}$ are treated as real quantities. The matrix elements of $\mathcal{R}^v, \mathcal{R}^a, \mathcal{R}^v$ and S^a for the down type

incoming quarks are the following

$$
\begin{aligned}
R^v_{11} &= \left[\left(a_1 - \frac{1}{2}b_1\right)\beta_w - b\left(\beta_w - \beta_i\cos\theta\right) + \frac{b}{2}\beta_w\right]\sin\theta \\
R^v_{12} &= \left[-2\left(2a_7 - b_7\right)\beta_w^2\gamma_w^2 - \left(a_6 - \frac{1}{2}b_6\right) + \frac{i}{2}\beta_i^2 b\right]\sin\theta \\
R^v_{13} &= -\frac{1}{2}\gamma_w\left[\left(2a_- - b_-\right)\beta_w\cos\theta + \beta_i\left(b_5\beta_w^2 + ib_6\right) + b\beta_i\beta_w\left(\beta_w - \beta_i\cos\theta\right)\right. \\
&\quad \left. -b\cos\theta\left(\beta_w - \beta_i\cos\right) - b\beta_i\sin^2\theta\right] \\
R^v_{22} &= \left[-\left(a_1 - \frac{1}{2}b_1\right)\beta_w + \frac{b}{2}\beta_w\right]\sin\theta \\
R^v_{23} &= -\frac{i}{2}\gamma_w\left\{b_-\beta_i\beta_w + \left[\left(2a_5 - b_5\right)\beta_w^2 + i\left(2a_6 - b_6\right)\right]\cos\theta + b\left[\beta_w\left(\beta_i - \beta_w\cos\theta\right)\right.\right. \\
&\quad \left.\left. +\beta_i\left(\beta_w - \beta_i\cos\theta\right)\right]\right\} \\
R^v_{33} &= \left[-\left(a_1 - \frac{1}{2}b_1\right)\beta_w\left(2\gamma_w^2 - 1\right) + 2\left(2a_2 - b_2\right)\beta_w^3\gamma_w^4 + \left(2a_3 - b_3\right)\beta_w\gamma_w^2\right. \\
&\quad \left. +\frac{b}{2}\beta_w\left(\frac{2\gamma_w^2}{\gamma^2} - 1\right) - b\gamma_w^2\left(\beta_w - \beta_i\cos\theta\right)\right]\sin\theta
\end{aligned}
\tag{2.14}
$$

$$
\begin{aligned}
R^a_{11} &= \left[-\frac{1}{2}b_1\beta_w - b\left(\beta_w - \beta_i\cos\theta\right) + \frac{b}{2}\beta_w\right]\beta_i\sin\theta \\
R^a_{12} &= \left[\frac{1}{2}\left(4b_7\beta_w^2\gamma_w^2 + b_6\right) + \frac{ib}{2}\right]\beta_i\sin\theta \\
R^a_{13} &= \frac{1}{2}\gamma_w\left[b_-\beta_i\beta_w\cos\theta + \left(2a_5 - b_5\right)\beta_w^2 + i\left(2a_6 - b_6\right) - b\left(\beta_w - \beta_i\cos\theta\right)^2 + b\beta_i^2\sin^2\theta\right] \\
R^2_{22} &= \frac{1}{2}\left(b_1 + b\right)\beta_w\beta_i\sin\theta \\
R^a_{23} &= \frac{i}{2}\gamma_w\left[\left(2a_- - b_-\right)\beta_w + \left(b_5\beta_w^2 + ib_6\right)\beta_i\cos\theta - b\beta_i\beta_w\left(\beta - \beta_w\cos\theta\right) - b\left(\beta_w - \beta_i\cos\theta\right)\right] \\
R^a_{33} &= \left[\frac{1}{2}b_1\beta_w\left(2\gamma_w^2 - 1\right) - 2b_2\beta_w^3\gamma_w^4 - b_3\beta_w\gamma_w^3 - \frac{1}{2}b\beta_w - b\gamma_w^2\left(\beta_w - \beta_i\cos\theta\right)\right]\beta_i\sin\theta
\end{aligned}
\tag{2.15}
$$

$$
\begin{aligned}
S^v_{11} &= \frac{1}{2\gamma_i}\left[-\beta_i b_1^S - (2a_1 - b_1)\,\beta_w\cos\theta - b\,(\beta_i - \beta_w\cos\theta) + 2b\beta_i^2\sin^2\theta\right] \\
S^v_{12} &= \frac{1}{2\gamma_i}\left\{\left[2a_6 - b_6 + 2\,(2a_7 - b_7)\,\beta_w^2\gamma_w^2\right]\cos\theta + 4b_3^S\beta_i\beta_w\gamma_w^2\right\} \\
S^v_{13} &= \frac{\gamma_w}{2\gamma_i}\left[(2a_- - b_-)\,\beta_w - 2b\,(\beta_w - \beta_i\cos\theta) + b\beta_w\right]\sin\theta \\
S^v_{22} &= \frac{1}{2\gamma_i}\left[\beta_i b_1^S + (2a_1 - b_1)\,\beta_w\cos\theta + b\,(\beta_i - \beta_w\cos\theta)\right] = -S^v_{11} + \frac{b}{\gamma_i}\beta_i^2\sin^2\theta \\
S^v_{23} &= -\frac{i\gamma_w}{2\gamma_i}\left[(2a_5 - b_5)\,\beta_w^2 + i\,(2a_6 - b_6) - b\beta_w^2\right]\sin\theta \\
S^v_{33} &= \frac{1}{2\gamma_i}\{\,\beta_i\left[b_1^S\left(2\gamma_w^2 - 1\right) - 4b_2^S\beta_w^2\gamma_w^4\right] + [\,(2a_1 - b_1)\left(2\gamma_w^2 - 1\right) \\
&\quad -4\,(2a_2 - b_2)\,\beta_w^2\gamma_w^4\,]\,\beta_w\cos\theta - 2\,(2a_3 - b_3)\,\gamma_w^2\beta_w\cos\theta \\
&\quad +b\left(2\gamma_w^2 - 1\right)(\beta_i - \beta_w\cos\theta) + 2b\gamma_w^2\,(\beta_w - \beta_i\cos\theta)\cos\theta\,\}
\end{aligned}
\tag{2.16}
$$

$$
\begin{aligned}
S^a_{11} &= -\frac{1}{2\gamma_i}\left[\left(4\gamma_z^2 - 1\right)b_8 + b_1^P\right] \\
S^a_{12} &= \frac{1}{2\gamma_i}\left[\left(4\beta_w\gamma_w^2 b_{10} - b_5\beta_w\right)\left(4\gamma_z^2 - 1\right) + 4\beta_w\gamma_w^2 b_3^P + b\,(\beta_w - \beta_i\cos\theta)\right] \\
S^a_{13} &= -\frac{i\gamma_w}{2\gamma_i}b\beta_i\beta_w\sin\theta \\
S^a_{22} &= -S^a_{11} \\
S^a_{23} &= -\frac{\gamma_w}{2\gamma_i}b\beta_i\sin\theta \\
S^a_{33} &= \frac{1}{2\gamma_i}\{\,\left[b_8\left(2\gamma_w^2 - 1\right) - 4b_9\beta_w^2\gamma_w^4 + 2b_4\beta_w^2\gamma_w^2\right]\left(4\gamma_z^2 - 1\right) \\
&\quad +b_1^P\left(2\gamma_w^2 - 1\right) - 4b_2^P\beta_w^2\gamma_w^4\,\}
\end{aligned}
\tag{2.17}
$$

where $\gamma_i, \gamma_w, \gamma_z, \beta_i, \beta_w, \beta_z$ are, as usual,

$$
\gamma_w = \sqrt{\frac{\hat{s}}{2m_w}} \qquad \beta_w = \sqrt{1 - \frac{4m_w^2}{\hat{s}}} \quad \text{etc .}
\tag{2.18}
$$

and $a_- = a_3 - ia_4, b_- = b_3 - ib_4$. For up-type quark, the density matrix is again given by equations (2.10) and (2.11) with the following changes. In eqs. (2.12a)(through t), (2.14), (2.15), (2.16) and (2.17), θ should be changed into $\pi - \theta$; the matrices $R^{v,a}, S^{v,a}$ should be transposed ($R, S \to \tilde{R}, \tilde{S}$); the signs of f_n^V for $n = 1,2,3,6,7$ should be flipped; the up-type quark masses in eq. (2.12a) should be substituted with the down-type quark masses and the down-type charges in eq. (2.12) should be substituted with the up-type charges.

Now we are ready to derive the cross sections. In the following section, we shall use $\hat{s}$ for the parton CM energy squared and s for the corresponding quantity of the incoming hadrons.

III. Formulas of W^+W^- Pair Production Cross Sections and Numerical Results

A. Formulas of W^+W^- Pair Production Cross Sections

From the density matrix, it is straightforward to obtain the corresponding differential cross section for polarized W^+ and W^- in the parton subprocess $q_i\bar{q}_i \to W^+W^-$:

$$\left(\frac{d\sigma}{d\cos\theta^*}\right)_{\lambda_1\lambda_2;\lambda_1'\lambda_2'} = \frac{\pi\alpha^2\beta_w}{4\hat{s}\beta_i}\tilde{P}_{\lambda_1\lambda_2;\lambda_1'\lambda_2'}\left(\theta^*, \sqrt{\hat{s}}\right) , \tag{3.1}$$

where θ^* is the angle between the W^- and the incoming hadron A in the hadron center of mass system. It follows from the factorization theorem for Drell-Yan processes [35] that the W^+W^- polarization cross section for $AB \to W^+W^-$ (where $A = P, B = \bar{P}$ for Tevatron) can be written as

$$\left(\frac{d\sigma}{dMd\cos\theta^* dy_+}\right)_{\lambda_1\lambda_2;\lambda_1'\lambda_2'} = \frac{\pi\alpha^2\beta_w}{sMN_c}\sum_j\left(\frac{1}{\beta_j^2}ch^2y_+ - sh^2y_+\right)\{ f_j^A\left(x_a, M^2\right) f_{\bar{j}}^B\left(x_b, M^2\right)$$

$$\tilde{P}_{\lambda_1\lambda_2\lambda_1'\lambda_2'}(\theta^*, M) + f_{\bar{j}}^A\left(x_a, M^2\right) f_j^B\left(x_b, M^2\right)\tilde{P}_{\lambda_1\lambda_2;\lambda_1'\lambda_2'}(\pi + \theta^*, M)\} , \tag{3.2}$$

where, $N_c = 3$ is the color factor; $j = u, c, t$ and d, s, b; $M = \sqrt{\hat{s}}$; $f_{j(\bar{j})}^A$ and $f_{\bar{j}(j)}^B$ are the parton distribution functions for parton $j(\bar{j})$ in A hadron and $\bar{j}(j)$ in B hadron and

$$y_+ = \frac{1}{2}(y_1 + y_2). \tag{3.3}$$

Here y_1 and y_2 are the rapidities, in the hadron CM frame, of W^- and W^+, and they are related to θ^* as follows

$$\beta_w \cos\theta^* = \tanh\frac{1}{2}(y_1 - y_2) \ . \tag{3.4}$$

The effects of the polarizations of W^+W^- can be seen through the correlations of their decay products. This has been discussed extensively by Hagiwara, et al. in Ref. 28, in the event when the masses of the final state fermions can be neglected. Although we shall discuss primarily the polarization cross sections as given in eq. (3.2), we give below the decay matrices for completeness.

Let $M_2(q_1,\lambda_1;p_1\sigma_1,p_2\sigma_2)$ be the amplitude for the decay of W^- into fermions of momenta p_1,p_2 and helicities σ_1,σ_2. Similarly, let $M_3(q_2,\lambda_2;p_3\sigma_3,p_4\sigma_4)$ be the corresponding quantity for W^+. We use θ_1,ϕ_1 to denote the polar and azimuthal angles of the down-type quark (lepton) in W^- decay and in the W^- rest frame. We use θ_3,ϕ_3 for the corresponding angles in W^+ decay (and in the W^+ rest frame). The decay matrix $D_{\lambda\lambda'}$ is defined by

$$D_{\lambda_1\lambda_1'} = \sum_{\sigma_1,\sigma_2} M_2\left(q_1\lambda_1;p_1\sigma_1,p_2\sigma_2\right) M_2^*\left(q_1\lambda_1';p_1\sigma_1,p_2\sigma_2\right) \tag{3.5}$$

$\bar{D}_{\lambda_2\lambda_2'}$ for W^+ decay is defined similarly. One can show that

$$D_{\lambda\lambda'} = \frac{e^2}{2\sin^2\theta_w} \mid V_{iI} \mid^2 c_-^2 \sum_{\sigma_1,\sigma_2} \left(p_1^o - \sigma_1 \mid \vec{p}_1 \mid\right)\left(p_2^o + \sigma_2 \mid \vec{p}_2 \mid\right) \ell_\lambda \ell_{\lambda'}^* , \tag{3.6}$$

where

$$\begin{aligned} \ell_\lambda \ &= \ < \cos\theta_1\cos\phi_1 + \frac{i}{2}(\sigma_1 - \sigma_2)\sin\phi_1, \\ &\qquad \cos\theta_1\sin\phi_1 - \frac{i}{2}(\sigma_1 - \sigma_2)\cos\phi_1, \ -\sin\theta_1 >_\lambda \ . \end{aligned} \tag{3.7}$$

Similarly,

$$\bar{D}_{\lambda\lambda'} = \frac{e^2}{2\sin^2\theta_w} \mid V_{iI} \mid^2 c_+^2 \sum_{\sigma_3,\sigma_4} \left(p_3^o + \sigma_3 \mid \vec{p}_3 \mid\right)\left(p_4^o - \sigma_4 \mid \vec{p}_4 \mid\right) \bar{\ell}_\lambda \bar{\ell}_{\lambda'}^* \ , \tag{3.8}$$

where

$$\bar{\ell}_\lambda \ = \ < \cos\theta_3\cos\phi_3 + \frac{i}{2}(\sigma_3 - \sigma_4)\sin\phi_3 \ ,$$

$$-\cos\theta_3\sin\phi_3+\frac{i}{2}(\sigma_3-\sigma_4)\cos\phi_3\ ,\sin\theta_3> \qquad (3.9)$$

In these formulas, c_-, c_+ are color factors and equal $1(\sqrt{3})$ for lepton (quark) final state. If we neglect the masses of the final state fermions, it is easily seen that $\sigma_1, \sigma_2, \sigma_3, \sigma_4$ can take only a particular value so that the summations over σ_i reduces to one term and we get the result of Ref. 28.

Equations (3.5), (3.8) can be combined with eq. (3.2) to give the complete cross sections for decay correlations. We shall postpone a detailed analysis of such correlations as was done in Ref. 28 for e^+e^- collisions, but rather analyze the polarization channels and the kinematical regions (θ^* and M) where a certain deviation from the Standard Model predictions is most easily found. For this purpose, we shall limit our discussions to the diagonal elements of eq. (3.2).

For given invariant mass m and the rapidity y_+ of the W^+W^- pair, the fractions x_a, x_b of hadron momenta carried by the incoming partons in hadron A and hadron B are fixed to be

$$x_a=\sqrt{\tau}\,(\beta_j\cosh y_+ +\sinh y_+)\,, x_b=\sqrt{\tau}\,(\beta_j\cosh y_+ -\sinh y_+)\,, \qquad (3.10)$$

here $\sqrt{\tau}=M/\sqrt{s}$.

We shall integrate over y_+ with the following cuts. Kinematically, it is constrained by $0\le x_a, x_b\le 1$. We put in the rapidity cuts of $\mid y_1 \mid\le 2.5, \mid y_2 \mid\le 2.5$ for W^- and W^+. Finally, since the mass of top quark is set at 70 GeV, which is comparable to the W mass, x_a and x_b for $t\bar{t}$ parton processes can be smaller than 10^{-4}, the limit of validity of the EHLQ structure functions which we are using. Moreover, so far as we know, there is still no completely satisfactory way of taking into account the heavy quark masses in the parton distribution functions [26,36]. To avoid the problem of small x, we put in the cuts $x_a, x_b\ge\tau$ which are satisfied automatically if the masses of the partons are neglected. Such cuts reduce the t-quark effective luminosity, but has very little effect on the luminosities of other quarks. At Tevatron energy, the differential cross sections are not sensitive to such cuts since the top luminosity is small anyway.

As pointed out above, taking $\lambda_1=\lambda_1', \lambda_2=\lambda_2'$, we have the polarized W^+W^- double differential cross section

$$\left(\frac{d\sigma}{dM d\cos\theta^*}\right)_{\lambda_1\lambda_2} =$$

$$\frac{\pi\alpha^2\beta_w}{3Ms}\sum_j \int dy_+ \left(\frac{1}{\beta_j^2}\cosh^2 y_+ - \sinh^2 y_+\right)\{ f_j^A\left(x_a, M^2\right) f_j^B\left(x_b, M^2\right) \tilde{P}^{(\theta^*,M)}_{\lambda_1\lambda_2;\lambda_1\lambda_2}$$

$$+ f_j^A\left(x_a, M^2\right) f_j^B\left(x_b, M^2\right) \tilde{P}_{\lambda_1\lambda_2;\lambda_1\lambda_2}\left(\pi+\theta^*, M\right)\} \qquad (3.11)$$

where the integration over y_+ is restricted by the kinematic cutoff we chose as explained above.

B. Numerical Results

In our numerical calculations, the EHLQ structure function (set 2, $\Lambda = 290\ MeV$) [26] is used and the parameters are chosen as follow

$$\begin{aligned} m_w &= 81.8\ GeV, \quad \sin^2\theta_w = 0.226, \quad \sqrt{S} = 2\ TeV \\ m_u &= 3\ MeV, \quad m_d = 5\ MeV, \quad m_s = 150\ MeV, \quad m_c = 1.5\ GeV, \quad m_b = 5.5\ GeV \\ m_t &= 70\ GeV, \quad M_H = 400\ GeV, \quad \Gamma_H = 30\ GeV\ . \end{aligned} \qquad (3.12)$$

The KMC matrix is taken to be

$$\begin{pmatrix} V_{ud}V_{us}V_{ub} \\ V_{cd}V_{cs}V_{cb} \\ V_{td}V_{ts}V_{tb} \end{pmatrix} = \begin{pmatrix} 0.975 & 0.222 & 0.00954 \\ 0.221 & 0.9644 & 0.1455 \\ 0.0231 & -0.144 & 0.9893 \end{pmatrix} \qquad (3.13)$$

Here we ignore the CP phase, but insist on unitarity.

The mass of the Higgs scaler (and that of H_p) are arbitrarily chosen to be 400 GeV with the corresponding width Γ_H [26] just to show a typical resonance behavior. As we shall find out, they have very little effect at Tevatron energy.

In order to see the various couplings' contributions, we plot our results according to the polarization channels and consider the anomalous $W^+W^-\gamma$ and $W^+W^-Z^o$ couplings separately. In order to facilitate comparison with the standard model, we plot our results of the standard model with solid line. One point which we

should note is that in the standard model we should consider the contributions from different flavors $i \neq j$ through the diagram, Fig. 4. However, due to the small KMC matrix mixing and/or the small quark mass difference, this mechanism, in fact, contributes little to the W^+W^- production at Tevatron energy. It is lower than others by at least an order of magnitude over the entire kinematical region we considered so that it can be safely ignored. In the figures, the numbers which accompany the dotted lines denote the corresponding coupling which deviates from the standard model by one unit and which contributes to the cross sections of the given channel as indicated in the Figure. In order to see the angle and energy dependences and to estimate the total events, we put the two graphs together in a Figure. We plot the angular distribution by taking the invariant mass of the W^+W^- pair equal to 0.3 TeV. On the other hand, we plot the dependence on the invariant mass of the W^+W^- production by taking a suitable angle to dramatize the variance with M changing.

In refs. [2–19, 29], the so-called "anomalous" moment κ_λ of W have been discussed a lot, which corresponds to the f_3^γ deviation. We also plot the λ_V term contributions, which are marked with λ in the Figs. The λ_V term is quite similar to the anomalous moment term. In space time representation, the anomalous moment term is $W_\mu^+ W_\nu V^{\mu\nu}$, but the λ_V term is $W_{\rho\mu}^+ W_\nu^\mu V^{\nu\rho}$, where W_μ is the vector potential of $W, W_{\mu\nu}$ and $V_{\mu\nu}$, are the field strength tensors of W and γ (or Z^o) respectively. They are related to the magnetic moment μ_w and the electric quadrupole moment Q_w of W by

$$\begin{cases} \mu_w = \frac{e}{2m_w} & (1 + \kappa_\gamma + \lambda_\gamma) \\ Q_w = -\frac{e}{m_w^2} & (\kappa_\gamma - \lambda_\gamma)\,. \end{cases} \tag{3.14}$$

In standard model, $\kappa_V = 1$ and $\lambda_V = 0$ at tree level. f_1, κ and λ are the only allowed form fectors if one insists on global SU(2) invariance upon switching off electromagnetism [24,31].

Owing to the relation in eq. (2.13), the magnitude of channels (12) and (21), (13) and (31), (23) and (32) are equal, hence, we plot only their sum. Similarly, as one can see from eqs. (2.14)–(2.17), the difference in (2.11) and (3.4) channels is down by a power of γ_w^2 compared to their sum so that we plot their sum only.

Finally, we note that Figures 5, 7, 9, 11 and 13 are for the form factors $f_i^\gamma (i =$

$1, \cdots, 7$) and Figures 6, 8, 10, 12 and 14 are for the form factors $f_i^z (i = 1, \cdots, 10)$.

IV. Discussions and Conclusions

By examining the figures, we can easily see the following features. Firstly, in standard model, the production cross section of W pairs in the central region (say $60^o \leq \theta^* \leq 120^o$) drop rapidly as the invariant mass M increase. The major contribution comes from the (12) transverse channel which originates from t–channel exchange diagrams. This rapid drop in cross section is, of course, the result of gauge cancellation as one expected from the standard moade. Next, we see that except for f_8 and f_{10}, an anomalous form factor of order 1 will increase the high mass W pair production cross section by at least an order of magnitude in the appropriately chosen θ^* region. This is usually the central region or near a dip in θ^* distribution. Finally, we notice that an anomalous f_i^z in general produce a larger deviation than an anomalous f_i^γ, but otherwise, with very similar θ^* and M distribution. This may make separating the contributions from f_i^z vs. f_i^γ difficult.

Now let us discuss each anomalous form factors [4] in the order of decreasing contributions to the high mass W pair production. From Figs. 9 and 10, we see that the contribution of an anomalous f_2 to (33) channel is greater than the corresponding standard model value by more than three orders of magnitude. Moreover, it keeps on increasing even when M reach 550 GeV. Tree level unitarity is badly broken and the γ_w^4 factor associated with f_2, as one can see from equations (2.14) and (2,15), overwhelms the decrease in parton luminosity as M is increased. The next in line are the form factors f_7 and λ. f_7 contributes to (12) channel only while λ contributes to (11), (22), (13) and (23) channels. Their contributions are more than two order of magnitudes above the standard model predictions for the transverse channels. The form factors f_4, f_5, f_6 contribute significantly only to the (13) and (23) channels. The deviations from the standard model predictions are large only for high mass ($> 300\ GeV$) W pairs and depend very much on the θ^* one chose. Note that the form factors f_3 and λ, for unit deviation from the standard model value, give the same contribution to (13) and (23) channels. f_3 also contributes to (11), (22), (33) channels as does f_1. Their contributions are more than one order of

[4] By anomalous, we mean unit deviations from the corresponding standard model values.

magnitude above the standard model values. Finally, among the three form factors f_8^z, f_9^z, f_{10}^z, only f_9^z contributes appreciably above the standard model predictions to the high mass W pair production cross section. Indeed its contribution to the (33) channel stays at about the same level for M increases from 200 to 500 GeV.

As for the form factors associated with the neutral scalar–vector boson couplings, we find that an order one deviation from the standard model value for these form factors produce, in most cases, no more than a factor of two increases in differential cross sections as is the case for f_8^z and f_{10}^z. This is expected as their contributions are suppressed by a factor of $(m_i/M)^2$, where m_i is the mass of the incoming fermions, while the probability of finding heavy quarks remain small for the values of M we considered at Tevatron energy. The contribution from f_9^z is helped by a factor of γ_z^4 which compensates for the decrease in heavy quark luminosity.

As noted before, in this paper, we discuss only the polarization cross sections for W^+W^- pair production. To proceed to the correlations of the decay products of the W^+W^- is straightforward and the numerical results will be presented elsewhere.

Now let us draw some conclusions based on the above discussion. At an integrated luminosity of 10 pb^{-1}, we expect, from standard model prediction, to see no high mass ($> 300\ GeV$) central ($60^o \leq \theta^* \leq 120^o$) W^+W^- pairs events. Any such event signals new physics. If the new physics are due to anomalous tri–vector boson couplings or Higgs–vector boson couplings which might arise, for example, from a new neutral gauge boson or neutral scalar, then our formalism can be applied to analyze such events. If the integrated luminosity can reach 100 pb^{-1}, we expect to see a few such events. They should come mainly from the (12) channel if standard model is correct.

It is very difficult to see at Tevatron energy any effects of the form factors whose contributions to the cross sections are proportional to the incoming quark masses. To test these form factors as well as to study in detail the polarization cross sections, one may have to wait forthe next generatin machines such as the SSC [32] or an upgraded high luminosity Tevatron.

V. Acknowledgements

We wish to thank E. Eichten and C. Quigg for valuable discussions, to thank Y. P. Yao for careful reading of the manuscript and useful comments and to thank W. K. Tung for some useful conversations. We would also like to thank the Theory Group of Fermilab for hospitality. One of the Authors (C.H.C) would like to thank Y. P. Yao and G. L. Kane for helpful discussions and the High Energy Physics Theory Group of the University of Michigan, as well as the Theoretical Physics Group of LBL, University of California at Berkeley, for hospitality during his visits there.

References

[1] UA1 Collaboration, Phys. Lett. **122B**, 103 (1983), **126B**, 398 (1982); UA2 Collaboration, Phys. Lett. **122B**, 476 (1983), **129B**, 130 (1983).

[2] T.D. Lee and C.N. Yang, Phys, Rev. **128**, 885 (1962).

[3] W.A. Bardeen, R. Gastmans and B. Lautrup, Nucl. Phys. **B46**, 319 (1972).

[4] W. Alles, Ch. Boyer and A.J. Buras, Nucl. Phys. **B119**, 125 (1977).

[5] F. Bletzacker and H.T. Nieh, Nucl. Phys. **B124**, 511 (1977).

[6] R. W. Brown and K.O. Miklaelian, Phys. Rev. **C1**, 259 (1979).

[7] K.J.F. Gaemers and G. J. Gounaris, Z. Phys. **C1**, 259 (1979).

[8] M. Gourdin and X.Y. Pham, Z. Phys. **C6**, 329 (1980).

[9] M. Hellmund and G. Ranft, Z. Phys. **C12**, 333 (1982).

[10] R.W. Robinett, Phys. Rev. **D28**, 1192 (1983).

[11] K.O. Mikaelian, M.A. Samuel and D. Sahdev, Phys. Rev. Lett. **43**, 746 (1979).

[12] J.D. Stroughair and C.L. Bilchak, Z. Phys. **C26**, 415 (1984).

[13] Zhu Dongpei, Phys. Rev. **D22**, 2266 (1980).

[14] M.A. Samuel, Phys. Rev. **D27**, 2724 (1983).

[15] R.W. Brown, K.L. Kowalski and S.J. Brodsky, Phys. Rev. **D28**, 624 (1983).

[16] C.L. Bilchak, R.W. Brown and J.D. Stroughair, Phys. Rev. **D29**, 375 (1984).

[17] B. Humpert, Phys. Lett. **135B**, 179 (1984).

[18] J. Stroughair and C.L. Bilchak, Z. Phys. **C23**, 377 (1984).

[19] C.L. Bilchak and J.D. Stroughair, Phys. Rev. **D30**, 1881 (1984).

[20] V. Barger, H. Baer, K. Hagiwara and R.J.N. Phillips, Phys. Rev. **D30**, 947 (1984).

[21] D.A. Dicus and K. Kallianpur, Phys. Rev. **D32**, 35 (1985).

[22] W.J. Stirling, R. Kleiss and S.D. Ellis, Phys. Lett. **163B**, 261 (1985).

[23] M. Tanimoto, Phys. Lett. **160B**, 312 (1985).

[24] M. Kuroda, J. Maalampi, D. Schildknecht and K.H. Schwarzer, BI–TP 86/27; BI–TP 86/12.

[25] J.F. Gunion and Z. Kunszt, Phys. Rev. **D33**, 665 (1986).

[26] E. Eichten, I. Hinchliffe, K. Lane and C. Quigg, Rev. Mod. Phys. **56**, 579 (1984); Erratum **58**, 1065 (1986).

[27] M.J. Duncan, G. L. Kane and W.W. Repko, Nucl. Phys. **B272**, 517 (1986).

[28] K. Hagiwara, R. D. Peccei, D. Zeppendfeld and K. Hikasa, Nucl. Phys. **B282**, 253 (1987).

[29] J. Cortes, K. Hagiwara and F. Herzog, Nucl. Phys. **B278**, 26 (1986).

[30] S.L. Glashow, Nucl. Phys. **22**, 579 (1961); S. Weinberg, Phys. Rev. Lett. **19**, 1264 (1967); A. Salam in Elementary particle theory, ed. N. Svartholm (Almquist and Wiksell, Stockholm, 1968), P.367.

[31] P.Q. Hung and J.J. Sakurai, Nucl. Phys. **B143**, 81 (1978); J.D. Bjorken, Phys. Rev. **D19**, 335 (1979); H. Fritzsch and G. Mandelbaum, Phys. Lett. **102B**, 319 (1981); L. Abbott and E. Farhi, Phys. Lett. **99B**, 69 (1981).

[32] Chao-Hsi Chang and S.-C. Lee, Fermilab-Pub-87/64-T, April, 1987.

[33] M.S. Chanowitz and M.K. Gaillard, Nucl. Phys. **B261**, 379 (1985); Phys. Lett. **142B**, 85 (1984); B.W. Lee, C. Quigg and H. Thacker, Phys. Rev. **D16**, 1519 (1977).

[34] S.D. Drell and T.M. Yan, Ann. Phys. (NY) **66**, 595 (1971).

[35] J. Frenkel, J.G.M. Gatheral and J.C. Taylor, Nucl. Phys. **B223**, 307 (1984); G. Bodwin, Phys. Rev. **D31**, 2616 (1985); J.C. Collins, D. Soper and G. Sterman, Nucl. Phys. **B261**, 104 (1985).

[36] J.C. Collins and W. K. Tung, Fermilab-Pub-86/39-T; H.E. Haber, D.E. Soper and R. M. Barnett, "Distributions of Heavy Particles in the Proton", SCIPP-86/70, 1986.

Figure Captions

Fig. 1: The three boson vertex. (a) VW^+W^- (b) $H_{Hp}W^+W^-$.

Fig. 2: The Feymann Diagrams for $q\bar{q} \to W^+W^-$
(a). The γ and z^o exchange diagram.
(b). The t-channel diagram.
(c). The scalar exchange diagram.

Fig. 3: $q\bar{q} \to W^+W^-$ process and its momentum assignment.

Fig. 4: Feymann diagram for $q_i\bar{q}_j \to WW(i \neq j)$.

Fig. 5: $\frac{d\sigma}{dmd\cos\theta^*}$ for (1,1) + (2,2) polarization channel; solid line is for standard model; dotted lines numbered by 1 and λ are for f_1^γ and $\lambda\gamma$ respectively with unit deviation from their standard model values.

Fig. 6: $\frac{d\sigma}{dmd\cos\theta^*}$ for (1,1) + (2,2) polarization channel; solid line is for standard model; dotted lines numbered by 1 and λ are for f_1^z, f_8^z andλz respectively with unit deviations from their standard model values.

Fig. 7: $\frac{d\sigma}{dmd\cos\theta^*}$ for (1,2) + (2,1) polarization channel; solid line is for standard model; dotted lines numbered by 6 and 7 are for f_6^γ and f_7^γ respectively with unit deviations from their standard model values.

Fig. 8: $\frac{d\sigma}{dmd\cos\theta^*}$ for (1,2) + (2,1) polarization channel; solid line is for standard model; dotted lines numbered by 6, 7 and 10 are for f_6^z, f_7^z and f_{10}^z respectively with unit deviations from their standard model values.

Fig. 9: $\frac{d\sigma}{dmd\cos\theta^*}$ for (3,3) polarization channel; solid line is for standard model; dotted lines numbered by 1, 2 and 3 are for f_1^γ, f_2^γ and f_3^γ respectively with unit deviation from their standard model values.

Fig. 10: $\frac{d\sigma}{dmd\cos\theta^*}$ for (3,3) polarization channel; solid line is for standard model; dotted lines numbered by 1, 2, 3, 4, 8 and 9 are for f_1^z, f_2^z, f_3^z, f_4^z, f_8^z and f_9^z respectively with unit deviations from their standard model values.

Fig. 11: $\frac{d\sigma}{dmd\cos\theta^*}$ for (1,3) + (3,1) polarization channel; solid line is for standard model; dotted lines numbered by 3, 4, 5, 6 and λ are for f_3^γ, f_4^γ, f_5^γ, f_6^γ and $\lambda\gamma$ respectively with unit deviations from their standard model values.

Fig. 12: $\frac{d\sigma}{dmd\cos\theta^*}$ for (1,3) + (3,1) polarization channel; solid line is for standard model; dotted lines numbered by 3, 4, 5, 6 and λ are for f_3^z, f_4^z, f_5^z, f_6^z and λz respectively with unit deviations from their standard model values.

Fig. 13: $\frac{d\sigma}{dmd\cos\theta^*}$ for (2,3) + (3,2) polarization channel; solid line is for standard model; dotted lines numbered by 3, 4, 5, 6, and λ are for f_3^γ, f_4^γ, f_5^γ, f_6^γ and $\lambda\gamma$ respectively with unit deviation from their standard model values.

Fig. 14: $\frac{d\sigma}{dmd\cos\theta^*}$ for (2,3) + (3,2) polarization channel; solid line is for standard model; dotted lines numbered by 3, 4, 5, 6 and λ are for f_3^z, f_4^z, f_5^z, f_6^z and λz respectively with unit deviations from their standard model values.

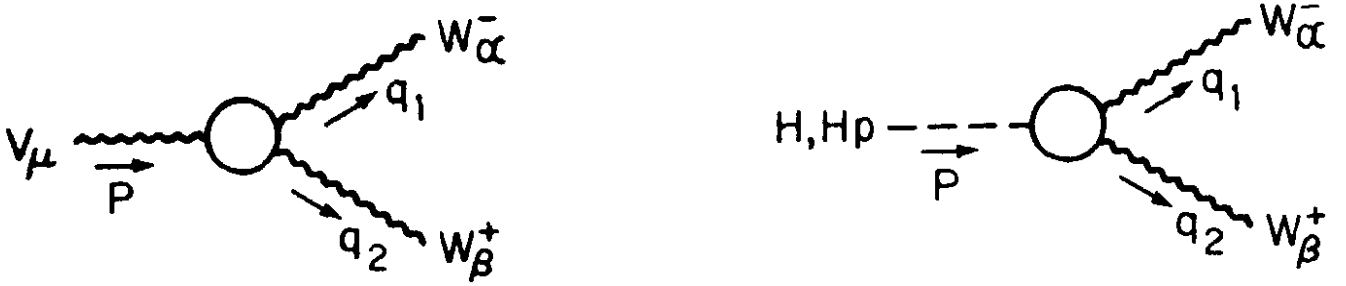

Fig. 1

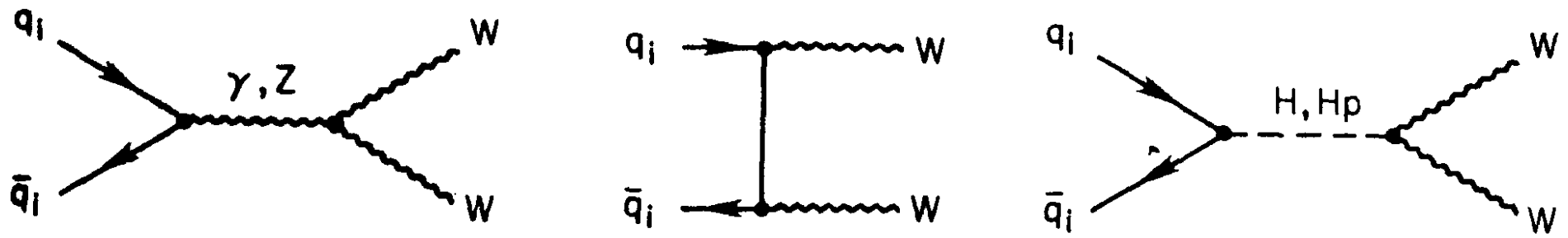

Fig. 2

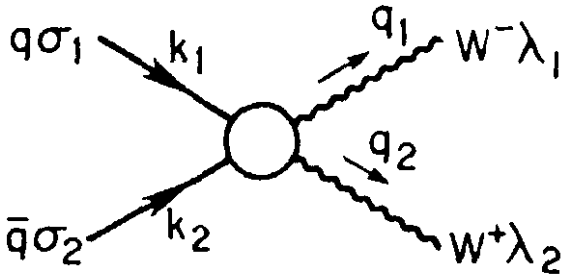

Fig. 3

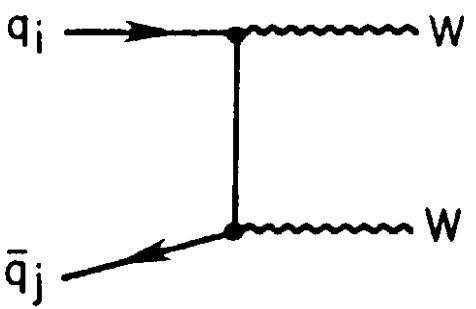

Fig. 4

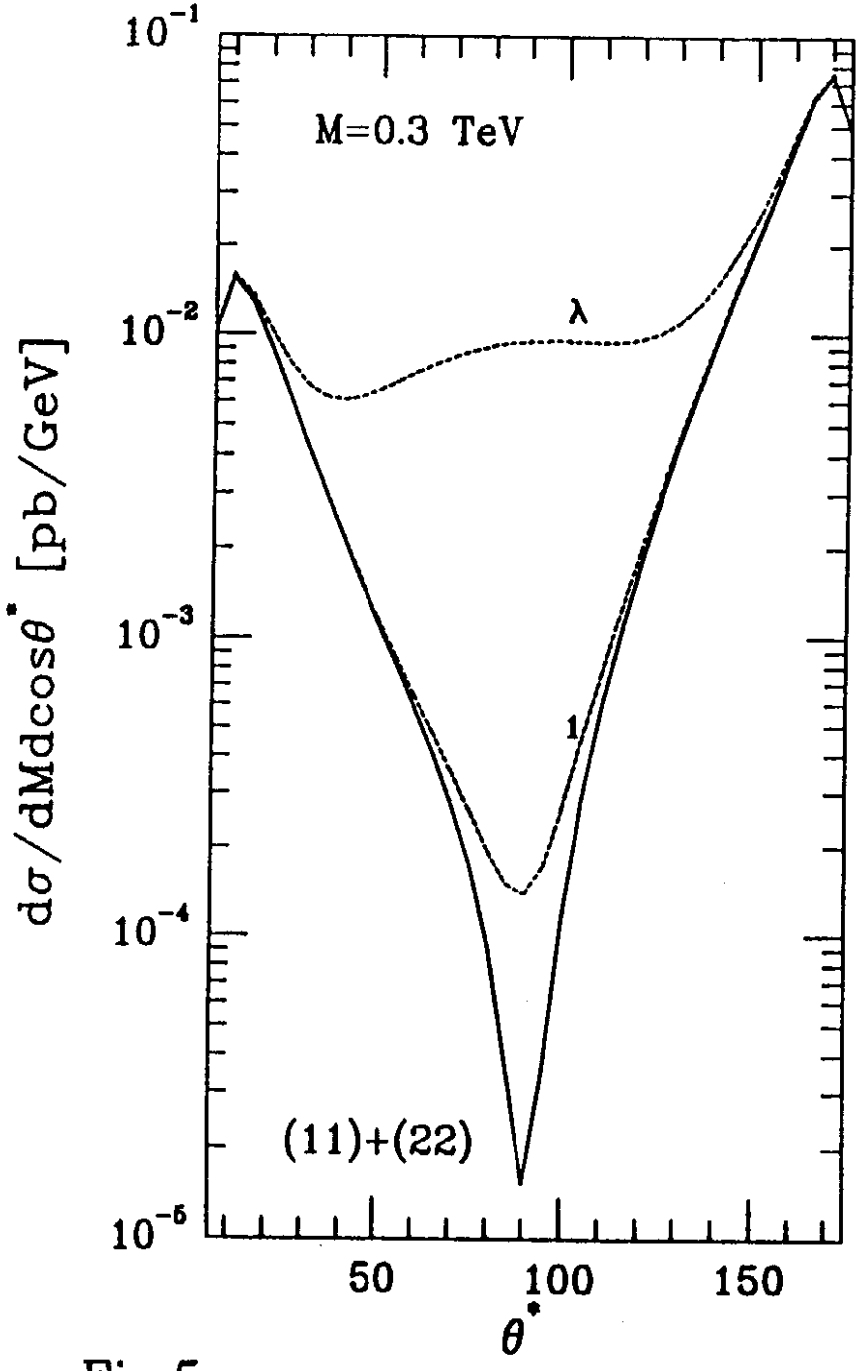

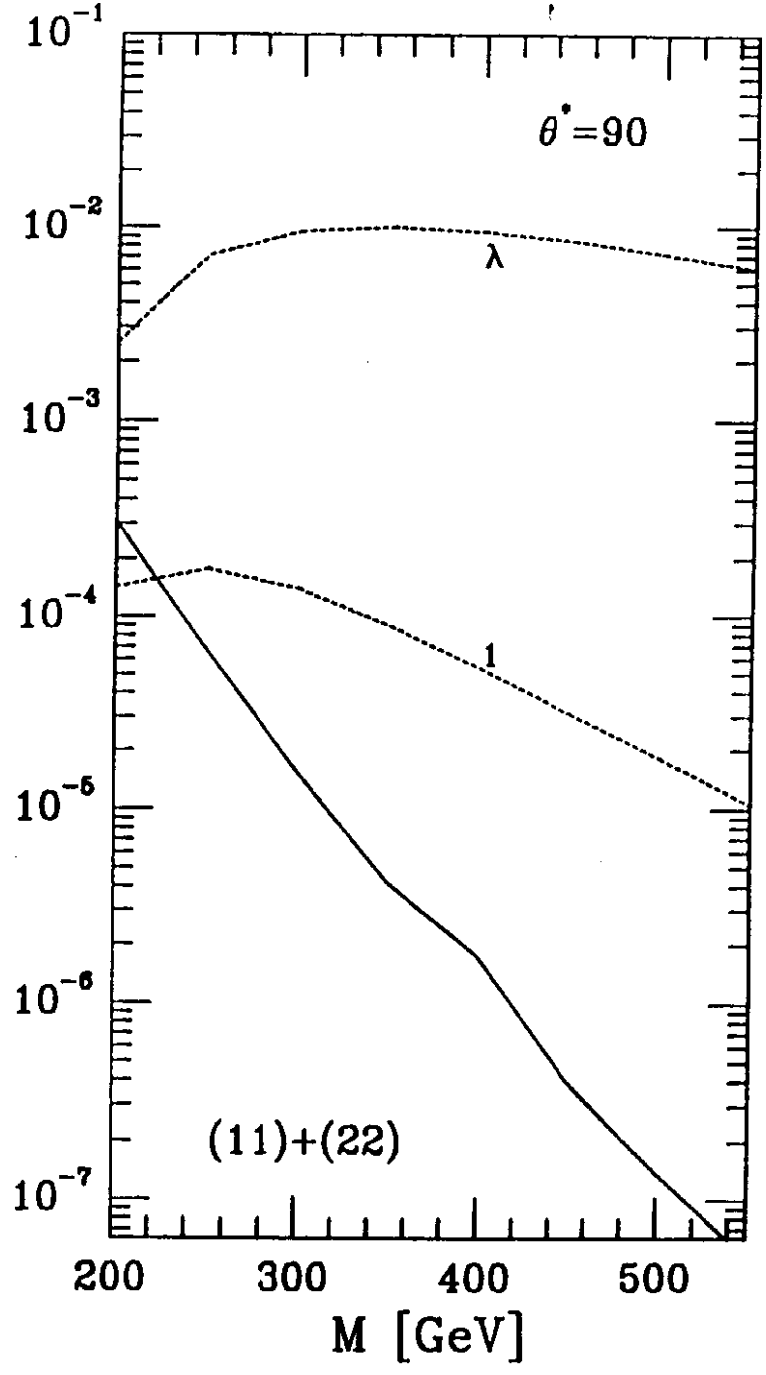

Fig.5

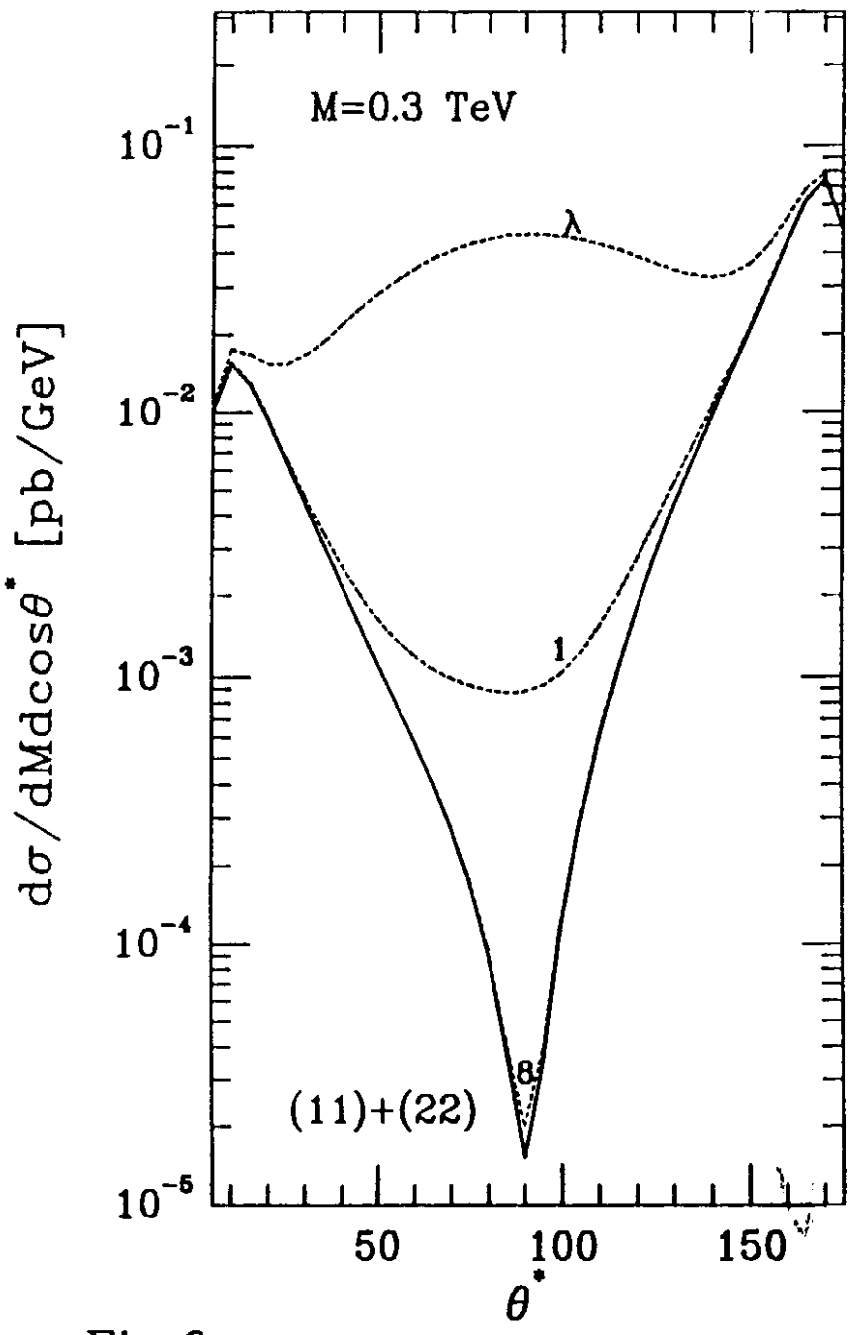
M=0.3 TeV
λ
1
8
(11)+(22)
10^{-1}
10^{-2}
10^{-3}
10^{-4}
10^{-5}
50
100
150
θ^*
$d\sigma/dMdcos\theta^*$ [pb/GeV]

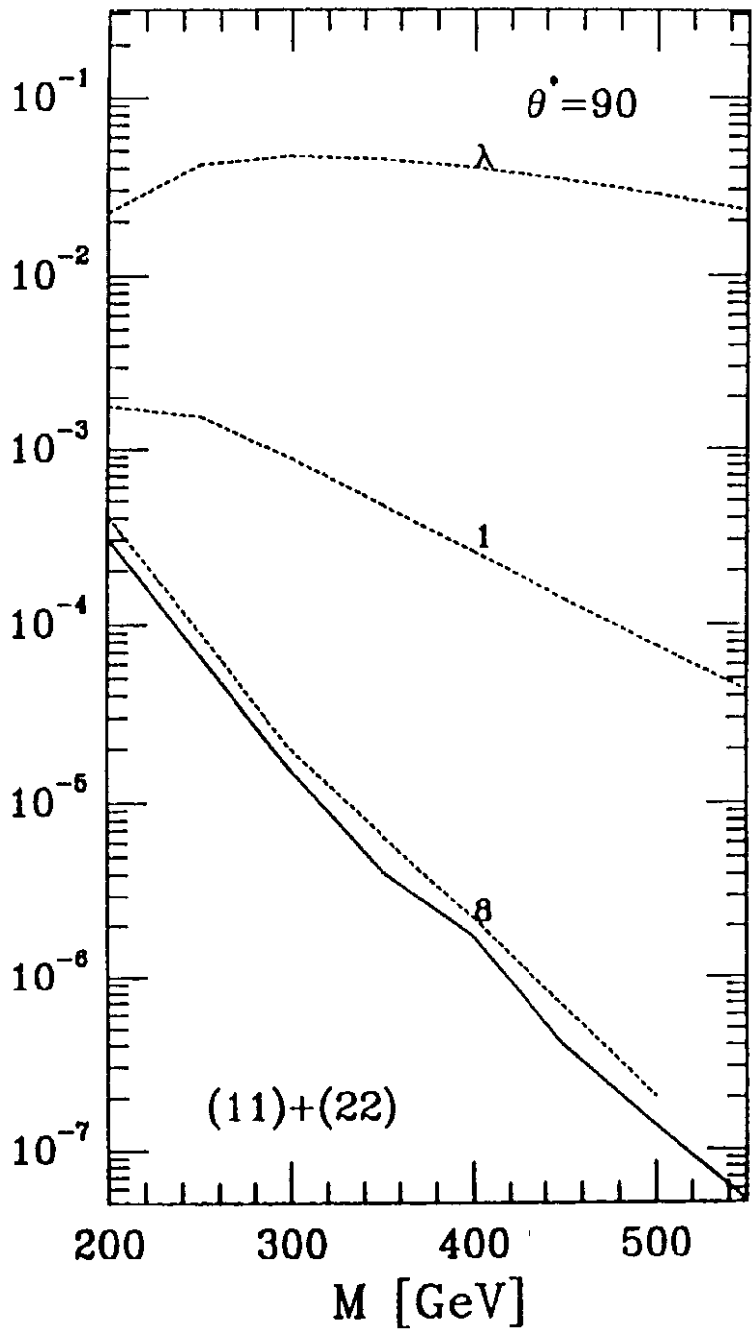
θ^*=90
λ
1
8
(11)+(22)
10^{-1}
10^{-2}
10^{-3}
10^{-4}
10^{-5}
10^{-6}
10^{-7}
200
300
400
500
M [GeV]

Fig.6

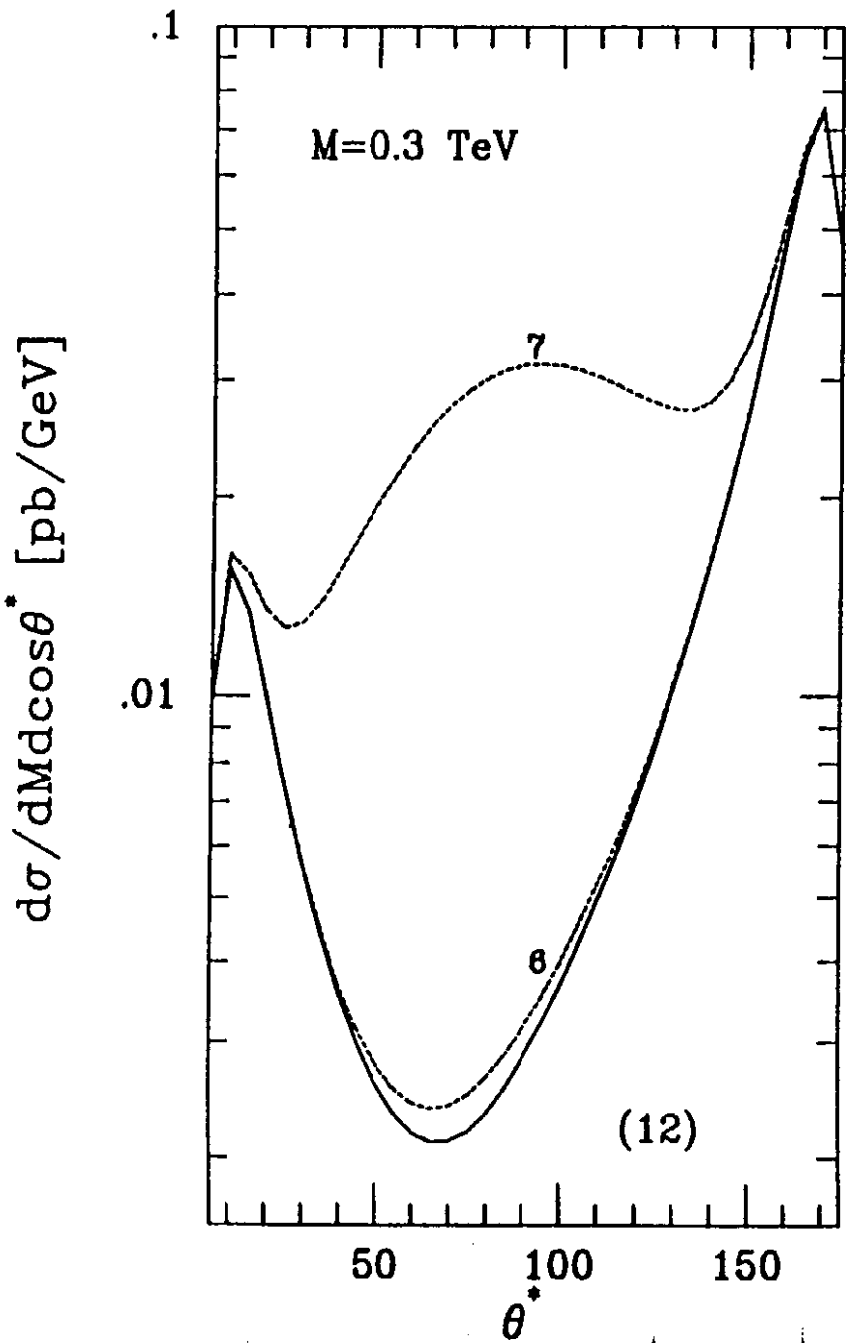
.1
M=0.3 TeV
7
.01
6
(12)
50
100
150
θ*
dσ/dMdcosθ* [pb/GeV]

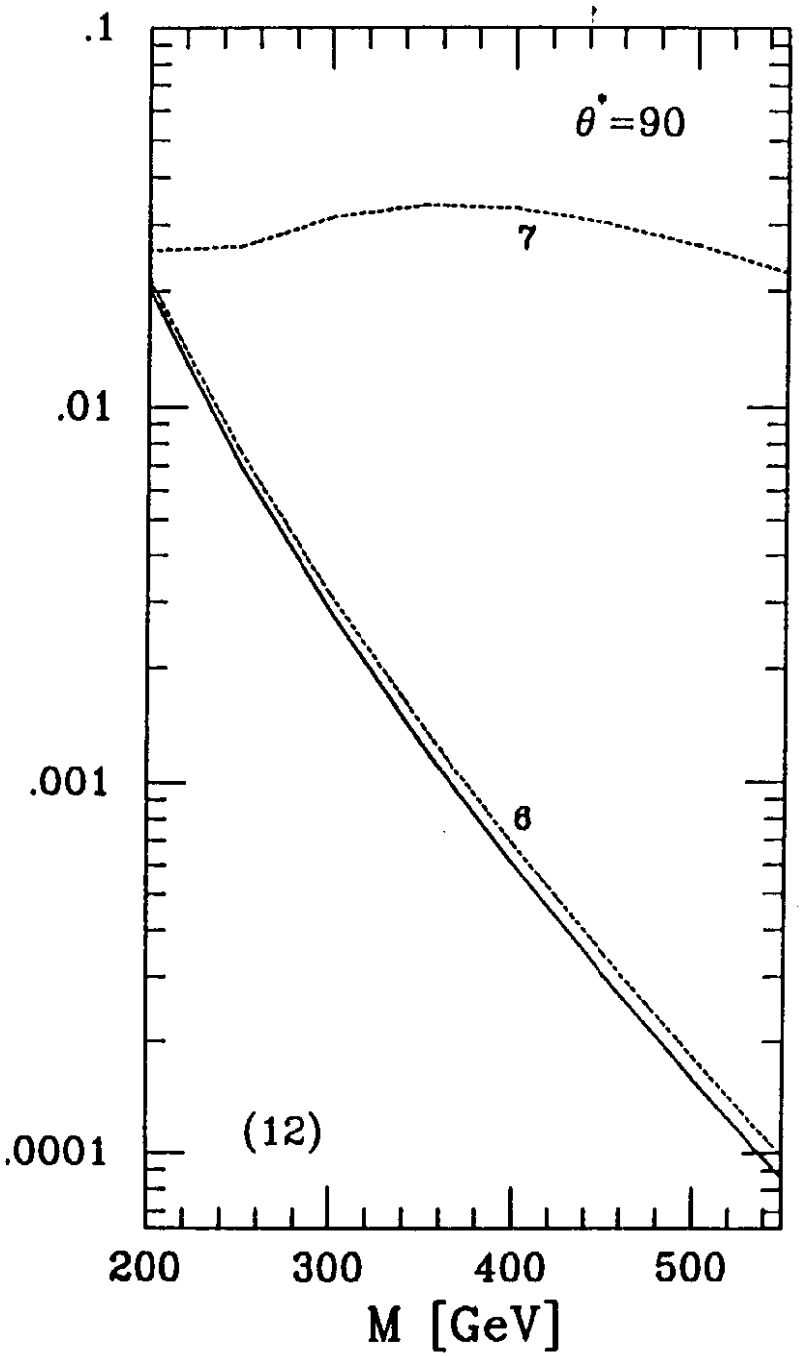
.1
θ*=90
7
.01
.001
6
.0001
(12)
200
300
400
500
M [GeV]

Fig.7

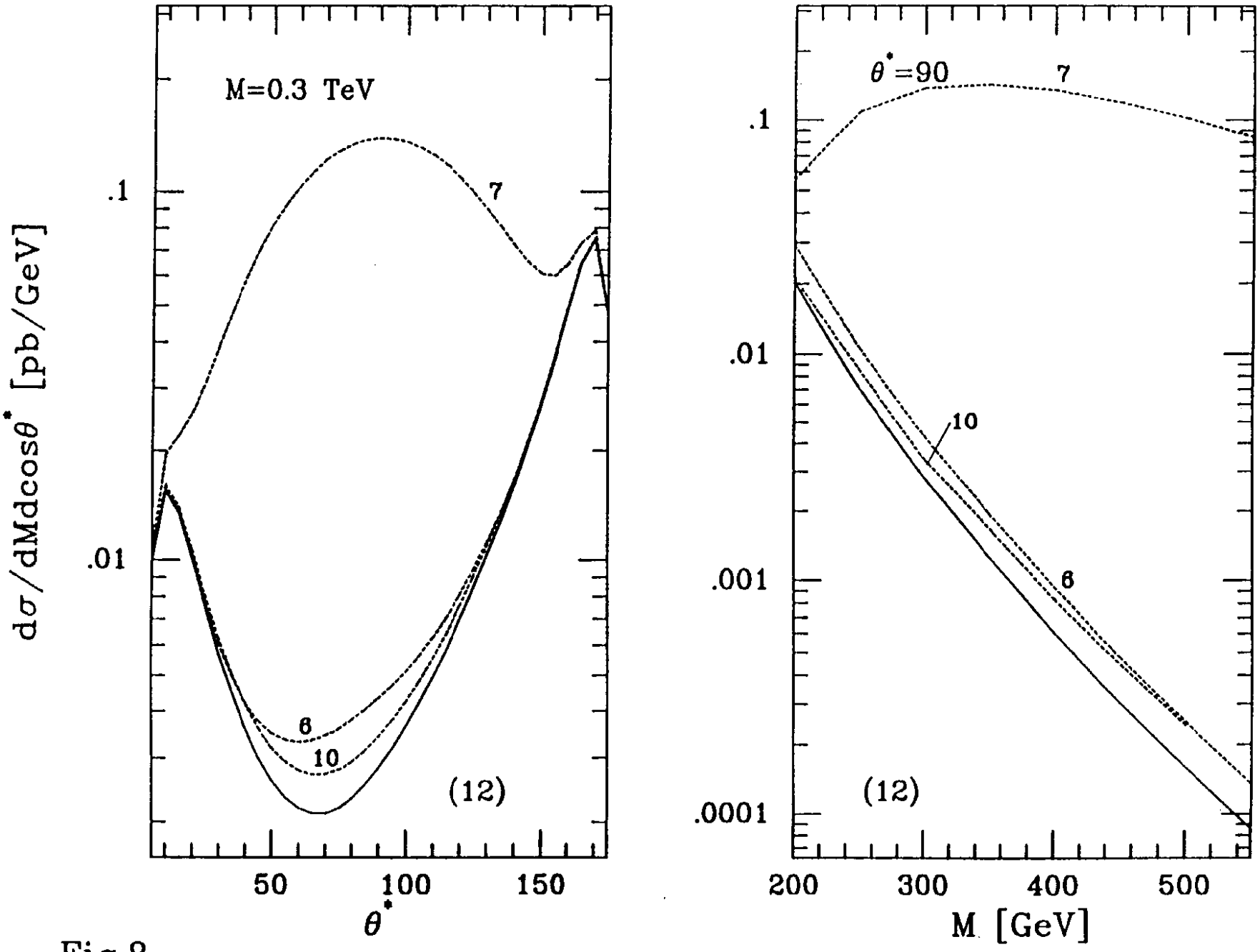
M=0.3 TeV
7
6
10
(12)
.1
.01
50
100
150
θ^*
$d\sigma/dMdcos\theta^*$ [pb/GeV]
θ^*=90
7
6
10
(12)
.1
.01
.001
.0001
200
300
400
500
M [GeV]

Fig.8

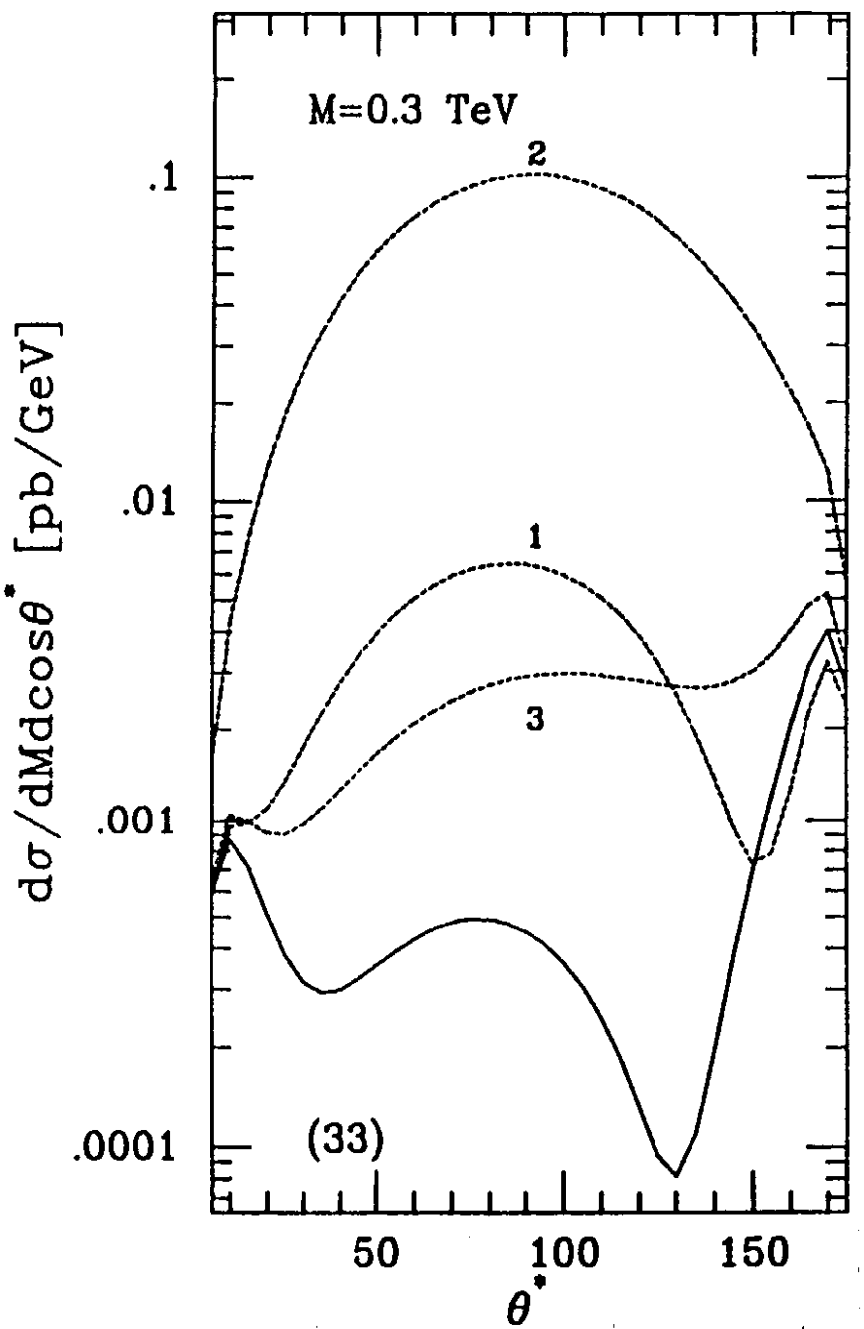
M=0.3 TeV
2
1
3
(33)
.1
.01
.001
.0001
50
100
150
θ*
dσ/dMdcosθ* [pb/GeV]

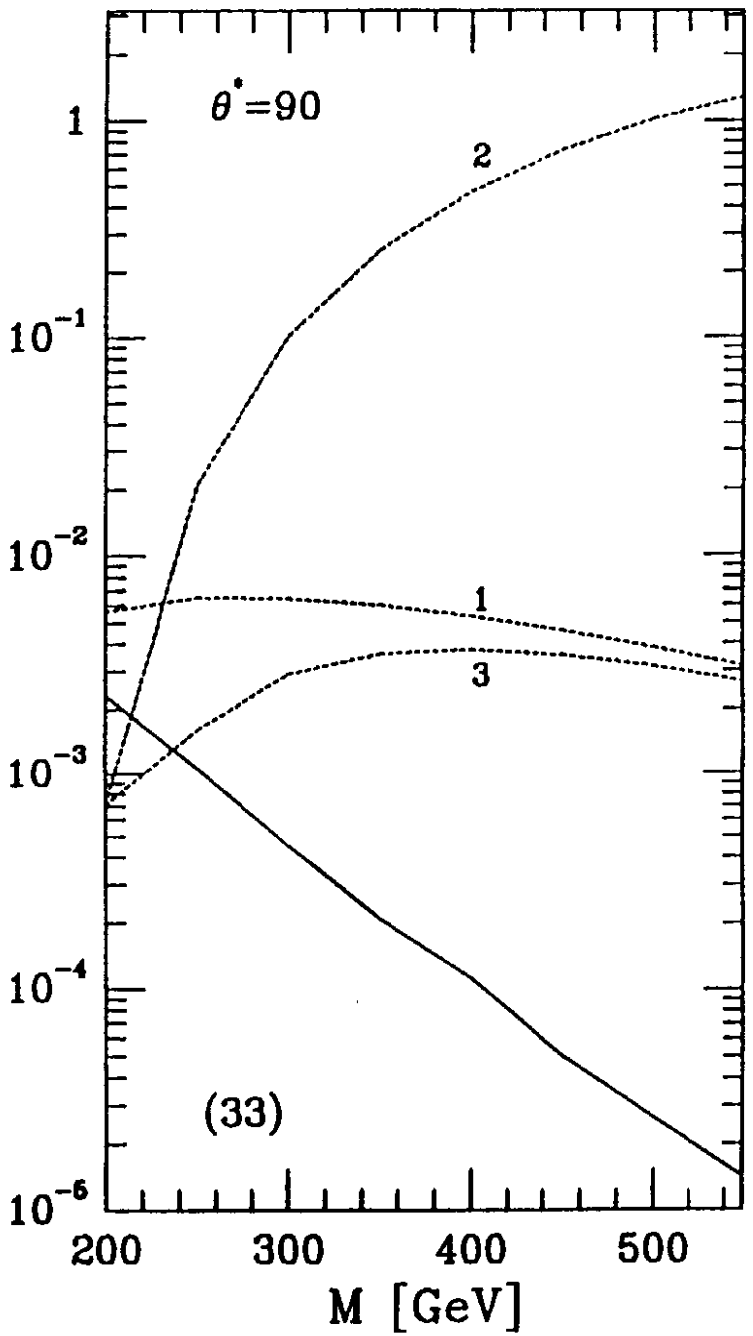
θ*=90
2
1
3
(33)
1
10⁻¹
10⁻²
10⁻³
10⁻⁴
10⁻⁵
200
300
400
500
M [GeV]

Fig.9

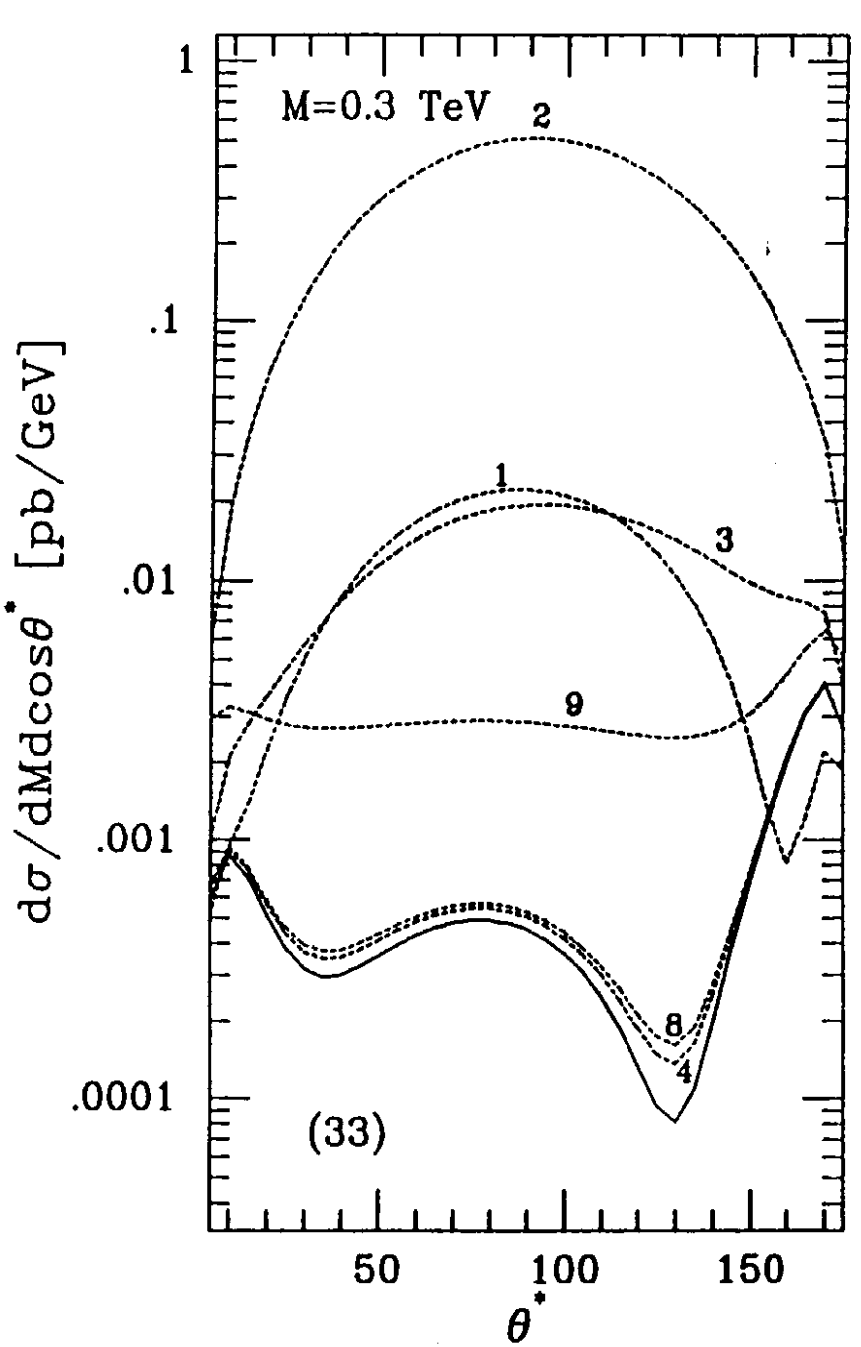
M=0.3 TeV
2
1
3
9
8
4
(33)
1
.1
.01
.001
.0001
50
100
150
θ*
dσ/dMdcosθ* [pb/GeV]

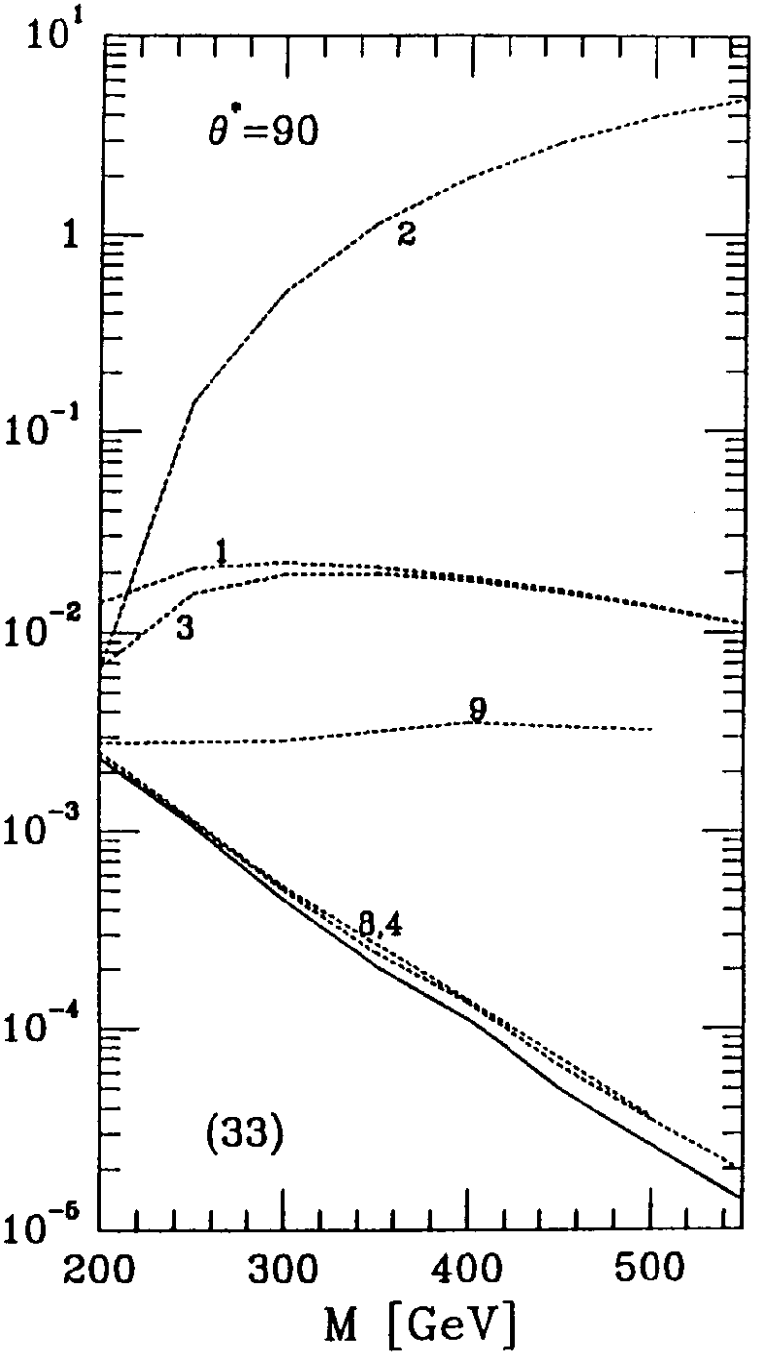
θ*=90
2
1
3
9
8,4
(33)
10¹
1
10⁻¹
10⁻²
10⁻³
10⁻⁴
10⁻⁵
200
300
400
500
M [GeV]

Fig.10

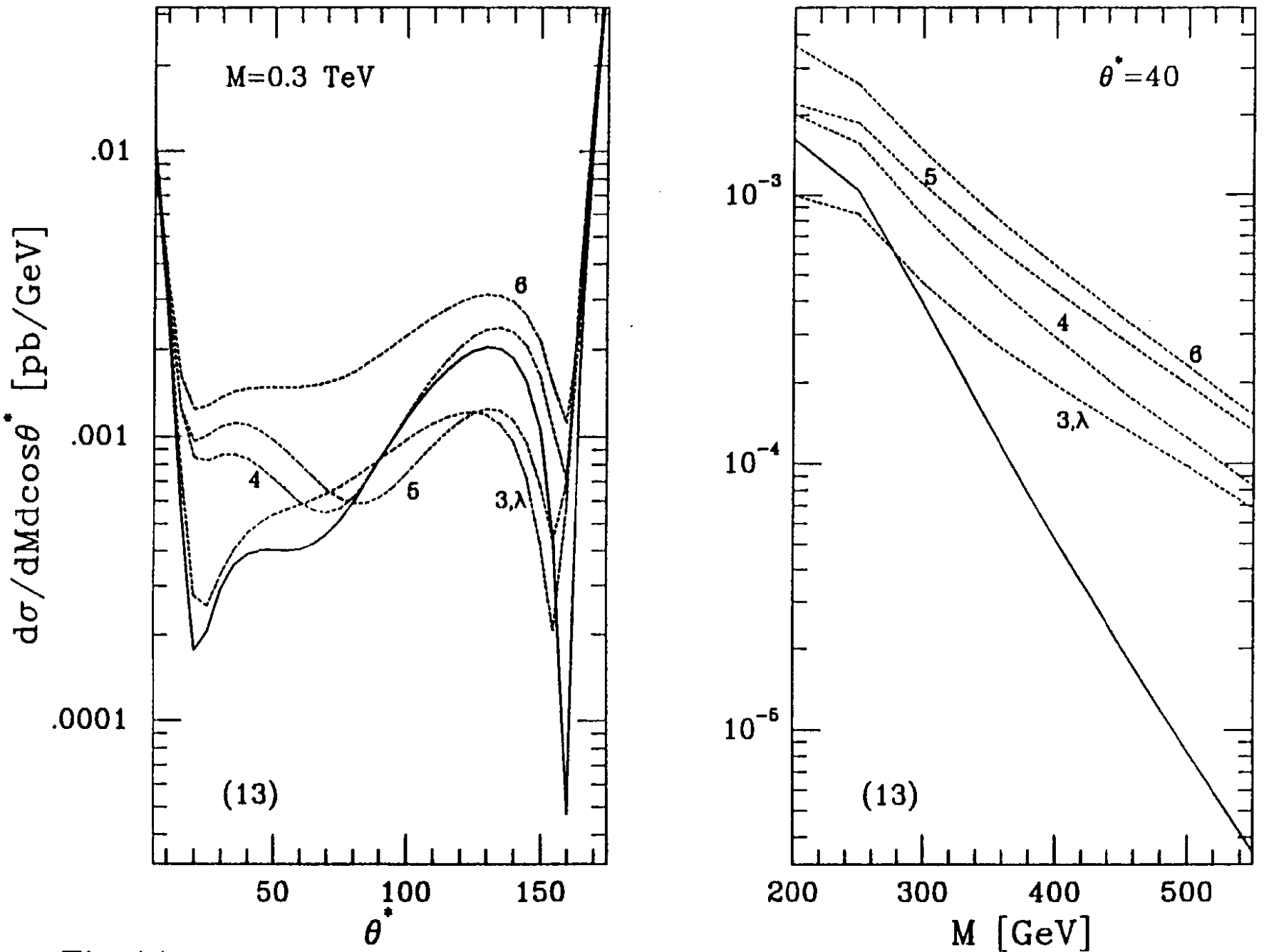
M=0.3 TeV
.01
.001
.0001
$d\sigma/dMd\cos\theta^*$ [pb/GeV]
6
4
5
3,λ
(13)
50
100
150
θ^*
θ^*=40
10^{-3}
10^{-4}
10^{-5}
5
4
6
3,λ
(13)
200
300
400
500
M [GeV]

Fig.11

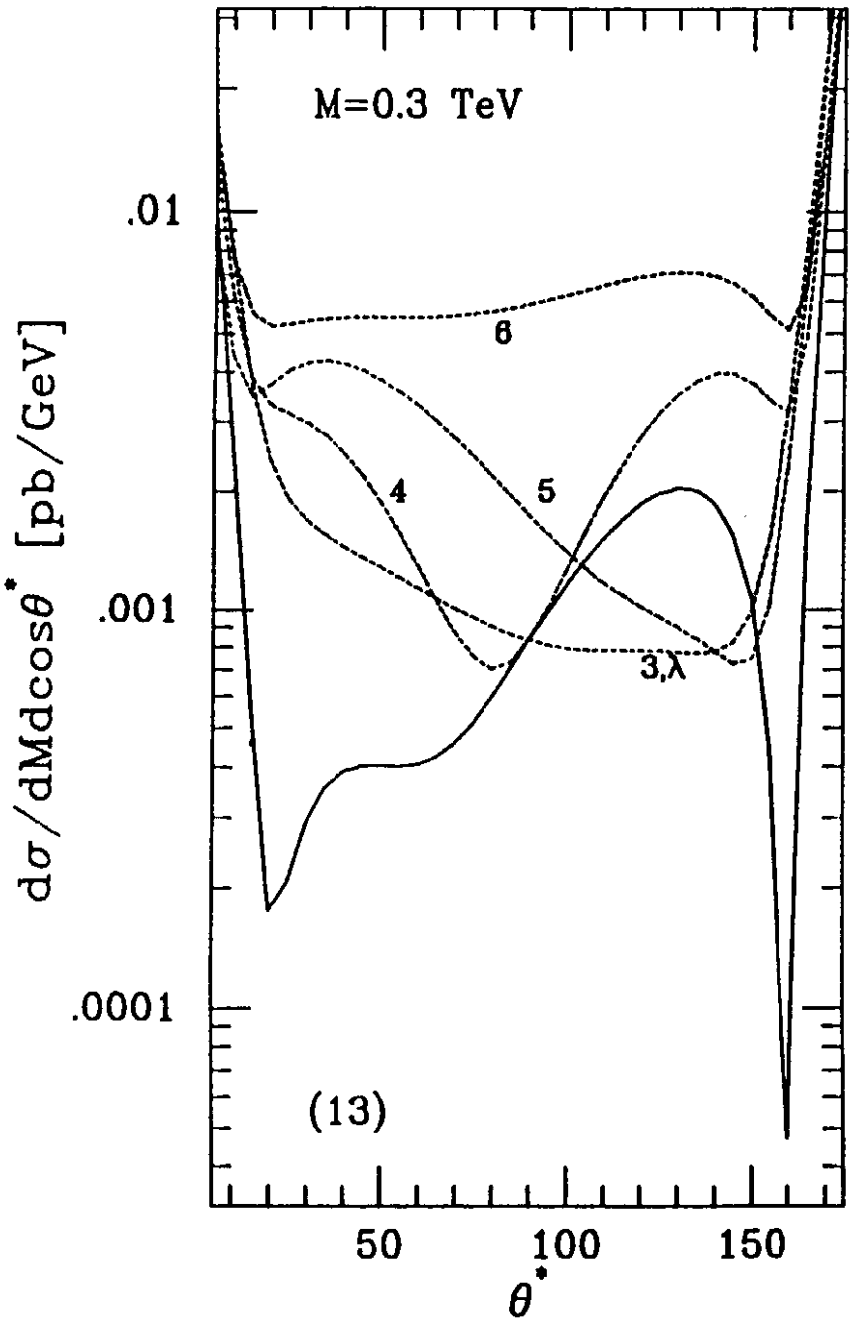
M=0.3 TeV
.01
.001
.0001
6
5
4
3,λ
(13)
50
100
150
θ*
dσ/dMdcosθ* [pb/GeV]

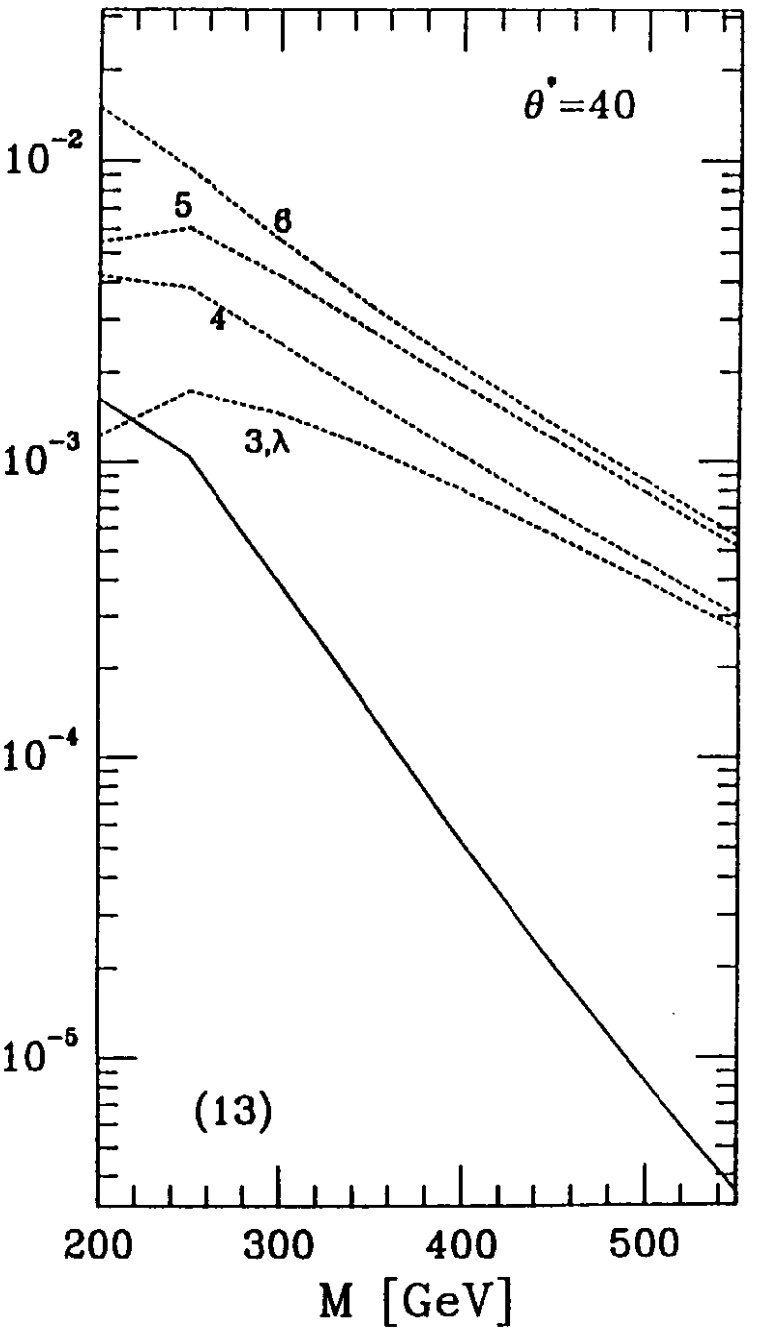
θ*=40
10^-2
10^-3
10^-4
10^-5
6
5
4
3,λ
(13)
200
300
400
500
M [GeV]

Fig.12

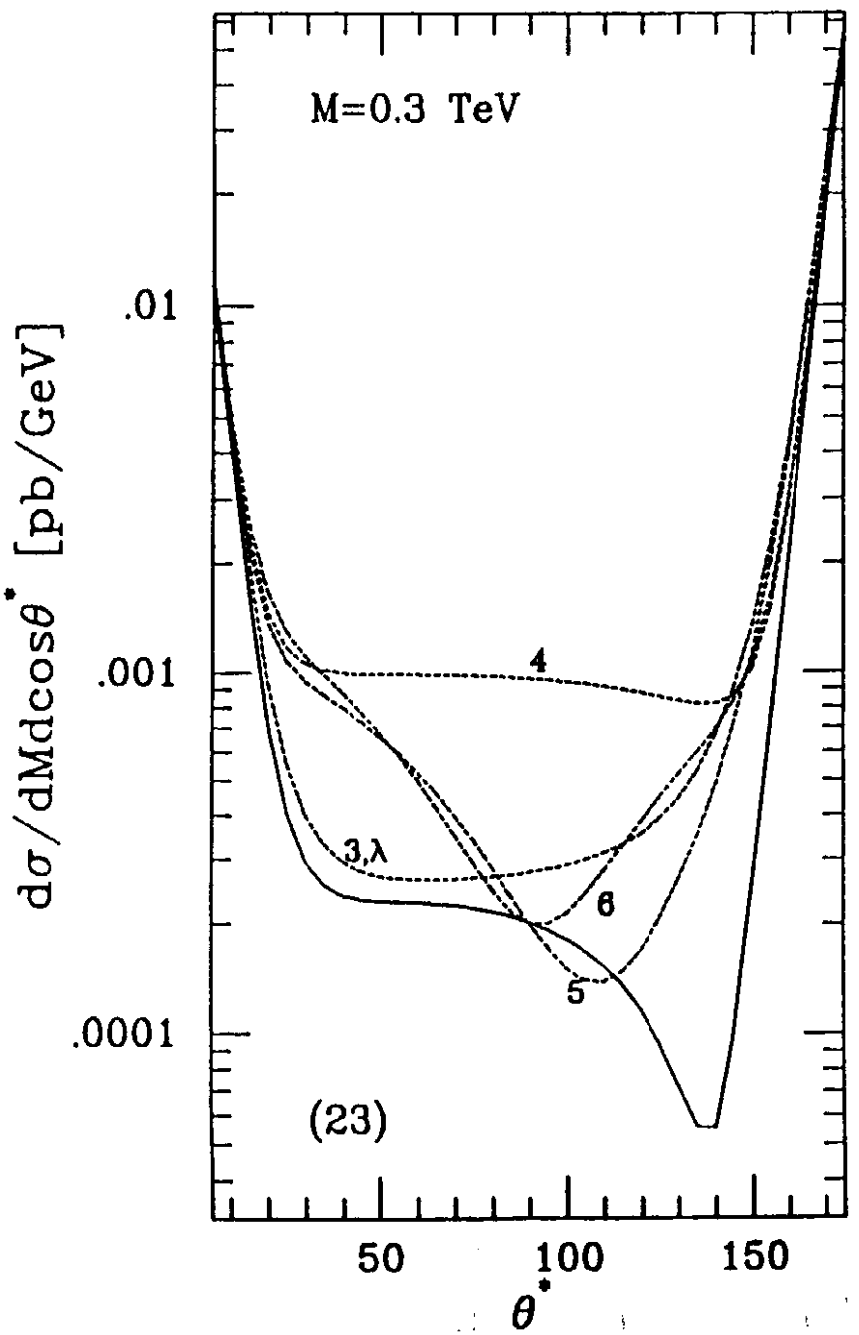
M=0.3 TeV
.01
.001
.0001
dσ/dMdcosθ* [pb/GeV]
4
3,λ
6
5
(23)
50
100
150
θ*

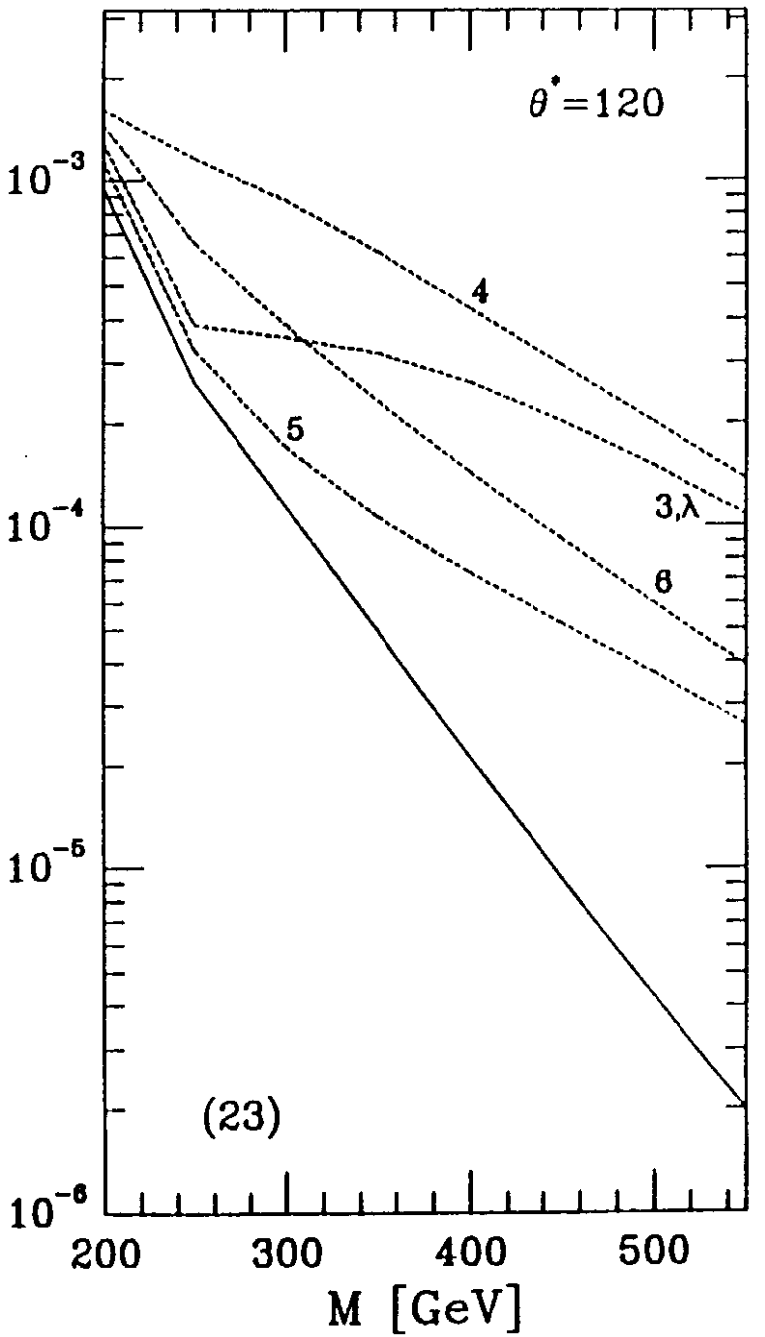
θ*=120
10⁻³
10⁻⁴
10⁻⁵
10⁻⁶
4
5
3,λ
6
(23)
200
300
400
500
M [GeV]

Fig.13

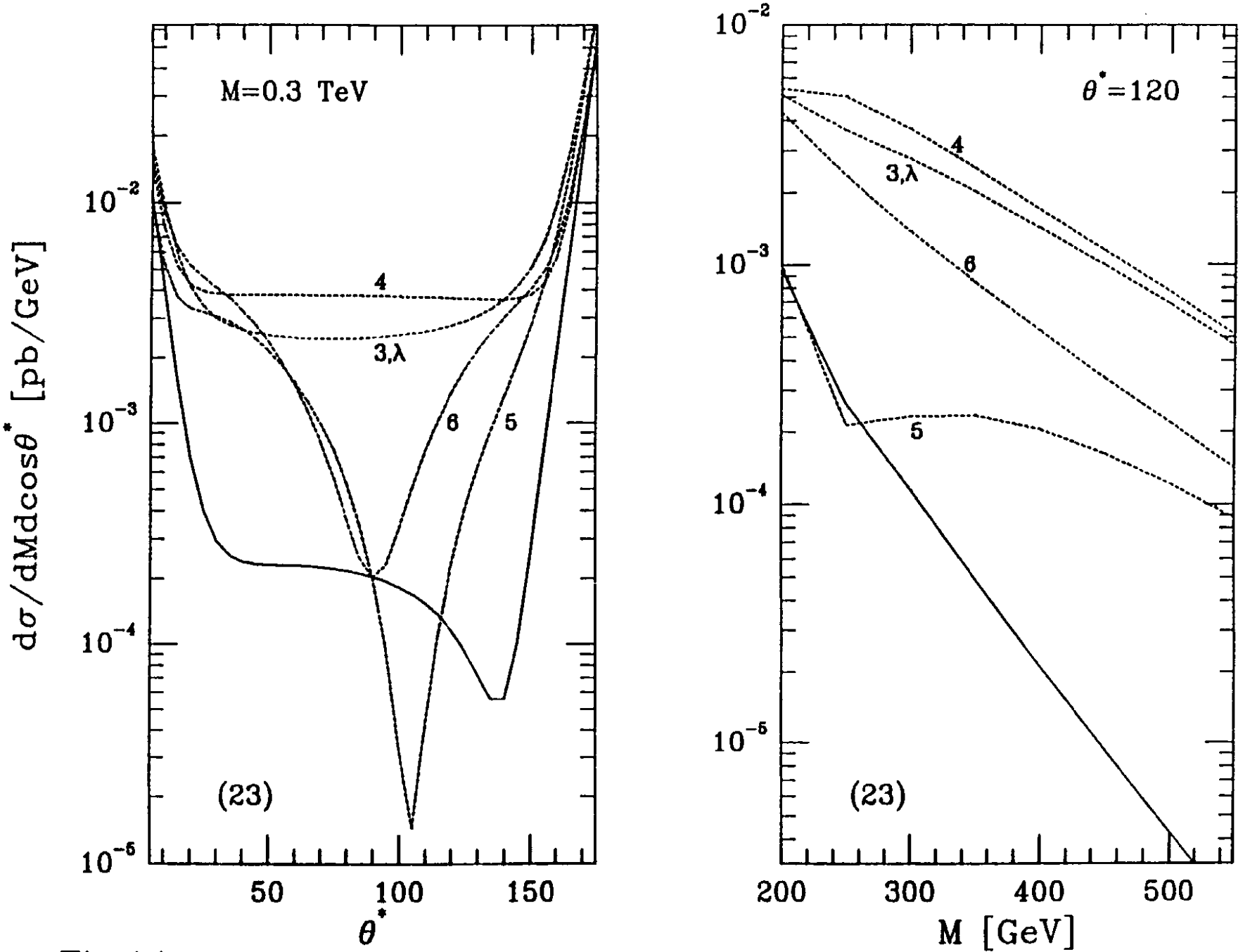
M=0.3 TeV
$d\sigma/dMd\cos\theta^*$ [pb/GeV]
10^{-2}
10^{-3}
10^{-4}
10^{-5}
4
3,λ
6
5
(23)
50
100
150
θ^*
θ^*=120
10^{-2}
10^{-3}
10^{-4}
10^{-5}
4
3,λ
6
5
(23)
200
300
400
500
M [GeV]

Fig.14